A functional interaction between TDP-43 and USP10 reveals USP10 dysfunction in TDP-43 proteinopathies

Marrero-Gagliardi A[1, #], Noda J[1, #], Zanovello M[2], Brito Armas JM[1], Bampton A[2], Torres P[3], Pérez Hernández C[1], Fumagallo F[1], Taoro L[1], Muñoz de Bustillo Alfaro R[1], Brown AL[2], Quinet G[4], Andrés-Benito P[5], Ferrer I[6], Acebes A[7], Freire R[4], Smits VAJ[4], Keuss M[2], Portero-Otin M[3], Lashley T[2], Fratta P[2], Acevedo-Arozena A[1*]

1. Canary Islands University Hospital Research Unit, ITB-ULL and CIBERNED, La Laguna, Tenerife, Spain
2. UCL Institute of Neurology, University College London, UK
3. Institute for Biomedical Research (IRB) Lleida, Spain
4. Canary Islands University Hospital Research Unit, ITB-ULL, Spain
5. Bellvitge Institute for Biomedical Research (IDIBELL), CIBERNED, L'Hospitalet de Llobregat, Spain.
6. Bellvitge Institute for Biomedical Research (IDIBELL), CIBERNED, L'Hospitalet de Llobregat, and Department of Pathology and Experimental Therapeutics, University of Barcelona, Spain.
7. University of La Laguna, ITB-ULL, Spain

# These authors contributed equally to this work

* Corresponding author: aacevedo@ull.edu.es

ABSTRACT

Amyotrophic lateral sclerosis (ALS) is a fatal neurodegenerative disorder characterised by the progressive degeneration of motor neurons in the cerebral cortex and spinal cord, with a rapid progression from diagnosis to death. The great majority of ALS cases and around 50% of FTD cases present with TDP-43 pathology, leading to mislocalization and cytoplasmic aggregation of TDP-43, which can result in both its loss of nuclear functions and a gain of toxicity in the cytoplasm. TDP-43 and other RNA-binding proteins accumulate in stress granules (SGs) under stress conditions. The ubiquitin-specific protease 10 (USP10) is an inhibitor of SGs assembly that has been recently linked to neurodegeneration. Here, we identified a new functional interaction between TDP-43 and USP10, in which USP10 can control multiple aspects of TDP-43 biology that are thought to play important roles in its involvement in disease pathogenesis, such as its cytoplasmic and nuclear aggregation, expression and splicing functionality. In turn, TDP-43 is also able to control diverse aspects of USP10 biology, such as its expression levels, aggregation and function. Critically, we found USP10 dysregulation in ALS and FTD patients, overall suggesting a possible role for USP10 in ALS/FTD pathogenesis.

INTRODUCTION

ALS is a fatal neurodegenerative disease characterised by the progressive degeneration of motor neurons in the cerebral cortex and spinal cord, with a rapid progression from diagnosis to death (Taylor et al., 2016), which shares genetic and pathological features with FTD. In fact, about 20% of people with ALS meet the clinical criteria for a diagnosis associated with FTD (Strong et al., 2017). Both diseases are linked at the genetic, clinical and pathological levels, with each presenting as one end of a spectrum of overlapping clinical symptoms that are thought to represent a broad and continuous neurodegenerative disorder (Ling et al., 2013) (Taylor et al., 2016). TDP-43, a ubiquitously expressed and predominantly nuclear RNA/DNA binding protein encoded by the *TARDBP* gene that is involved in multiple aspects of RNA processing through its RNA binding capacity (Coyne et al., 2017) (Buratti, 2021), is thought to play a central role in ALS and FTD pathogenesis as one of the main components of the proteinaceous inclusions that pathologically define the great majority of ALS and up to 50% of FTD cases (Neumann et al., 2006) (Taylor et al., 2016). TDP-43 pathology, occurring when TDP-43 is depleted from the nucleus and sequestered as hyperphosphorylated insoluble aggregates in the cytoplasm, perikarya, and/or dystrophic neurites of affected neurons, is also present in all cases of the dementia entity limbic-predominant age-related TDP-43 encephalopathy (LATE) and up to 50% of Alzheimer's cases, that together with other disorders where TDP-43 pathology occurs, are collectively known as TDP-43 proteinopathies. It is generally accepted that in TDP-43 pathology, the cytoplasmic aggregation of TDP-43 confers a loss of nuclear function causing pleiotropic defects including in splicing regulation such as the expression of toxic cryptic exons (Mehta et al., 2023), as well as a possible gain of toxic function due to its cytoplasmic mislocalization that can in turn also contribute to the further nuclear clearance of TDP-43 and other RNA binding proteins (Vanden Broeck et al., 2015) (Ederle & Dormann, 2017) (Cook & Petrucelli, 2019) (Gasset-Rosa et al., 2019).

TDP-43 and other RNA binding proteins (RBPs) involved in ALS such as FUS are known to be components of stress granules (SGs), that are membraneless macromolecular ribonucleoprotein cytoplasmic condensates that are formed in response to different cellular stress conditions. Although the function of SGs is not clear, they are thought to promote cell survival under stress conditions by storing stalled translation components, including mRNAs, RBPs, ribosomal components and initiation factors (Ivanov et al., 2019) (Wolozin & Ivanov, 2019) (Advani & Ivanov, 2020). For their formation, SGs are thought to require an increase in intracellular free RNA concentrations to promote the condensation of the core SG protein G3BP1 (Kedersha et al., 2016) (Yang et al., 2020). Interestingly, TDP-43 controls *G3BP1* levels through direct mRNA binding, modulating SG formation (McDonald et al., 2011) (Aulas et al., 2012) (Aulas & Vande Velde, 2015). A key protein in the regulation of SG assembly is the ubiquitin-specific peptidase 10 (USP10), that inhibits SG formation by negatively influencing G3BP1 cooperativity via direct binding, in an interaction with G3BP1 that is mutually exclusive with that of Caprin1, that promotes SG formation (Panas et al., 2015) (Panas et al., 2015) (Hofmann et al., 2021) (Sheehan et al., 2022). USP10 is a multifaceted protein with several major cellular roles that could be either, dependent on its enzymatic deubiquitinase activity, including controlling the levels of critical proteins like p53 or AMPK

(Yuan et al., 2010), or independent of its activity, such as the inhibition of SG formation (Kedersha et al., 2016) (Yang et al., 2020).

Recently, USP10 has been linked to different neurodegenerative conditions. In AD, USP10 has been observed colocalizing with TAU aggregates in patients, and is thought to promote TAU aggregation in neuronal cells exposed to stress (Piatnitskaia et al., 2019). In cellular models of TDP-43 proteinopathy, USP10 has been shown to promote the elimination of TDP43-positive SGs under conditions of proteasome inhibition, whilst USP10 downregulation promotes the accumulation of TDP-43 insoluble fragments in the cytoplasm (Takahashi et al., 2022). Moreover, USP10 was identified as a modifier of C9Orf72 toxicity in *Drosophila* (K.-H. Lee et al., 2016).

Here, using different cellular models of TDP-43 cytoplasmic mislocalization to search for aggregation suppressors, we initially found that USP10 inhibits the formation of TDP-43 cytoplasmic inclusions through a mechanism that requires USP10 interaction with G3BP1. We then went on to study the effects of USP10 in modulating different aspects of TDP-43 biology, including its expression and splicing functionality. Moreover, we found that TDP-43 is also able to control different aspects of USP10 biology, including its expression, that we report to be misregulated in ALS and FTD patients, further implicating USP10 in ALS/FTD pathogenesis.

RESULTS

USP10 controls TDP-43 aggregation

To test the effect of USP10 on the cytoplasmic aggregation of TDP-43, we used different cellular models to get TDP-43 out of the nucleus and into the cytoplasm and to force its aggregation (Fig. 1A).

In the first model, we transfected different cell lines (HeLa, U2OS and SH-SY5Y) with a construct (GFP-TDP43$^{\Delta NLS}$) carrying a GFP-tagged TDP-43 harbouring mutations in its nuclear localization signal (NLS), leading to its mislocalization and the formation of cytoplasmic aggregates (Zhang et al., 2013). This method allowed us to model the production of TDP-43 cytoplasmic inclusions, the cardinal feature of TDP-43 proteinopathies such as ALS and FTD, and to test the effects of modulating USP10 expression on TDP-43 aggregation process. Co-transfection of GFP-TDP43$^{\Delta NLS}$ with USP10 caused a major decrease in both the numbers as well as the size of TDP-43 cytoplasmic inclusions ($p<0.001$ for both) in HeLa cells when compared to the effects of GFP-TDP43$^{\Delta NLS}$ alone (Fig. 1B, C). To ensure that these results were not dependent on the cell type, we performed the same experiments in U2OS and SH-SY5Y cell lines. Similarly to HeLa cells, co-transfection of GFP-TDP43$^{\Delta NLS}$ with USP10 caused a major decrease in the area ($p<0.001$ in U2OS and SH-SY5Y), as well as a lower number of cells with TDP-43 inclusions ($p<0.01$ in U2OS and $p<0.05$ in SH-SY5Y) in both cell lines when compared to GFP-TDP43$^{\Delta NLS}$ alone (Fig. S1. A, B).

We obtained the opposite effect after USP10 downregulation with siRNA. In U2OS cells, USP10 levels were first downregulated with siRNAs against *USP10* or Luciferase as a negative control, and then co-transfected with GFP-TDP43$^{\Delta NLS}$ with inclusion size and numbers quantified. USP10 downregulation caused a major increase in the size of TDP-43 inclusions

when co-transfected with GFP-TDP43$^{\Delta NLS}$ without affecting TDP-43 inclusion numbers compared to the transfection of GFP-TDP43$^{\Delta NLS}$ alone (Fig. 1D, E).

Given that different RBPs associated with ALS (including TDP-43) accumulate in SGs (Markmiller et al., 2018) (Fang et al., 2019) and knowing that USP10 interacts with G3BP1, the core protein of the SG-forming complex, such that USP10 inhibits SG assembly (Kedersha et al., 2016) (Yang et al., 2020), we wondered whether the effects of USP10 on TDP-43 aggregation might be mediated by USP10's role in regulating SG formation, as at least in this Hela model, the colocalization between TDP-43 and SGs was very high (Fig. S2.A). To address this, we co-transfected HeLa cells with GFP-TDP-43$^{\Delta NLS}$ and USP10 and quantified GFP-TDP43 inclusions as well as SGs by immunocytochemistry using G3BP1 antibodies. As expected for a known inhibitor of SG formation, USP10 co-transfection with GFP-TDP-43$^{\Delta NLS}$, led to a clear reduction in SG size and a decrease in the number of cells with SGs when compared with the co-transfection with the EV (Fig. 1F, G). This reduction in both the size and number of SGs after USP10 overexpression, is very similar to the effect observed on TDP-43 aggregates, suggesting that, at least in this Hela model that leads to a very high co-localization between SGs and TDP-43 cytoplasmic inclusions, TDP-43 aggregation clearance mediated by USP10 could be mediated by its effects as an inhibitor of SG formation. However, the model relies on the transfection of a GFP-tagged TDP43 that in itself leads to SG formation.

Thus, to better understand if the effects of USP10 on TDP-43 aggregation depend on SG formation, we used two different cellular models in which endogenous TDP-43 aggregation is induced by stress leading to the formation of at least some TDP-43 foci that do not colocalize with SG (Fig. 1A).

As a second cellular model, we used an already published inducible cellular model in U20S cells where the endogenous *TARDBP* gene is edited to harbour a disrupted NLS and a fluorescent tag (TDP-43$^{\Delta NLS}$-Clover) expressed under a doxycycline inducible system (Gasset-Rosa et al., 2019). 24 hours after doxycycline induction, which keeps TDP-43 in the cytoplasm without forming defined TDP-43 inclusions, we induced TDP-43 aggregation using previously reported oxidative stress conditions ($NaAsO_2$ 250 µM during 80 minutes). In this context, SG and TDP-43 foci were both formed and were completely independent (Fig. S2A), allowing us to assess the effects of USP10 specifically on endogenous TDP-43 aggregates that do not co-localize with SGs. Crucially, in this model, after induction of TDP43 cytoplasmic inclusions with doxycycline and stress, USP10 overexpression also led to a decrease in the number of TDP-43 inclusions per cell when compared to the EV control ($p>0.01$) (Fig. 1H, I). Thus, USP10 can also modulate TDP-43 aggregation independently of stress granule formation.

As the third cellular model, we treated SH-SY5Y cells with a combination of oxidative and osmotic stress based on previous reports (Y.-B. Lee et al., 2021), consisting in the incubation with 500 µM sodium arsenite for 40 minutes, followed by a treatment with 600 mM sorbitol for 40 minutes, and allowing the cells to recover for 1 hour with fresh media before the analysis. This treatment caused both the partial clearance of TDP-43 from the nucleus and its cytoplasmic aggregation concomitantly with stress granule formation. Under these stress conditions, again, SG and endogenous TDP-43 inclusions were both formed, but this time with a fraction of TDP-43 foci colocalizing and another not colocalizing with SG, further allowing us to assess the effects of USP10 on TDP-43 foci formation independently of SG. In this paradigm, USP10 overexpression caused a decrease in the area of TDP-43 inclusions ($p<0.005$)

when compared to the EV control (Fig. 1J, K), confirming that USP10 can modulate TDP-43 aggregation also independently of stress granule formation.

Next, we assessed if USP10 could also modulate endogenous TDP-43 aggregation in the nucleus (Ederle & Dormann, 2017) (Gasset-Rosa et al., 2019) via immunocytochemistry in HeLa cells transfected with USP10. As in the cytoplasm, USP10 overexpression reduced the number per cell of both endogenous TDP-43 nuclear foci (Fig. S1.C) or those induced by stress (500 µM NaAsO2 during 30 minutes) (Fig. S1.D). Thus, USP10 modulates TDP-43 aggregation in a variety of different contexts.

The effect of USP10 on TDP-43 cytoplasmic aggregation is independent of its deubiquitinase activity, but dependent on its binding to G3BP1

USP10's deubiquitinase activity is known to be critical in its involvement in regulating different cellular processes (Pickart, 2001) (Clague et al., 2013) (Yuan et al., 2010) (Liu et al., 2011). However, USP10 is also known to have critical functions that are independent of its catalytic activity, including in the regulation of SG formation (Kedersha et al., 2016) (Yuan et al., 2010) (Liu et al., 2011). Thus, to begin to determine the mechanisms by which USP10 inhibits TDP-43 aggregation, we used the GFP-TDP43$^{\Delta NLS}$ model in HeLa cells and tested the effects of a mutated version of USP10 devoid of its catalytic activity (USP10^{C424A}) (Bomberger et al., 2009) (He et al., 2021). Interestingly, the results show that enzymatically inactive USP10^{C424A} led to a decrease in TDP-43 aggregation that is indistinguishable from that of USP10 wild type (WT) (Fig. 2 A, B). Co-transfection of GFP-TDP43$^{\Delta NLS}$ with USP10^{C424A} caused a decrease in the area of TDP-43 inclusions ($p<0.001$), as well as a lower number of cells with TDP-43 inclusions ($p<0.001$) when compared to the EV.

Having ruled out the requirement of USP10's deubiquitinase activity for the inhibition of TDP-43 aggregation at least in this model, we continued our search for a mechanistic understanding of its effects on TDP-43. USP10 function as an inhibitor of SG formation is known to be mediated by its interaction with G3BP1 mediated through USP10 N-terminal domain. To test for a possible role of this interaction on USP10´s capacity to clear TDP-43 aggregates, we used a USP10^{F10A} mutant that loses its ability to bind G3BP1 through a FGDF motif in the N-terminus of USP10 (Panas et al., 2015) and co-transfected it with the GFP-TDP43$^{\Delta NLS}$ construct in HeLa cells. As already published in other contexts (Kedersha et al., 2016), in our model, the transfection of USP10^{F10A} had no effect on SG formation (Fig. 2A), validating the effects of the mutation. In terms of its effects on TDP-43 aggregation, USP10^{F10A} had no effects on TDP-43 aggregation, unlike the co-transfection with USP10^{Wt} or USP10^{C424A}, suggesting that the inhibitory role of USP10 in the formation of TDP-43 aggregates is mediated by its interaction with G3BP1 (Fig. 2A, B). However, in this cellular model, all TDP-43 cytoplasmic aggregates co-localize with G3BP1. Thus, to test the effects of USP10^{F10A} on TDP-43 aggregation independently of its colocalization with SG, we used the U2OS TDP-43$^{\Delta NLS}$-Clover inducible model treated with arsenite. Interestingly, in this model, USP10^{F10A} expression also had no effect on the number TDP-43 foci, unlike the USP10^{C424A}, that was able to reduce TDP-43 aggregates when compared to the EV control ($p<0,001$) (Fig. 2C, D). Overall, these results show that USP10 binding of G3BP1 is required for its inhibition of TDP-43 aggregation in a manner that it not dependant on TDP-43 colocalization with SGs.

USP10 regulates TDP-43 protein levels

Having established that USP10 can modulate TDP-43 aggregation, we went on to determine whether USP10 might be also regulating TDP-43 levels. We began by measuring the effects of overexpressing or downregulated USP10 on endogenous TDP-43 levels via immunoblots in U2OS cells. We found no differences in TDP-43 protein upon USP10 overexpression (Fig. 3A); however, USP10 downregulation caused a small but significant reduction on TDP-43 protein when compared to the siRNA control (Fig. 3B) ($p<0,05$), without affecting *TARDBP* mRNA levels (Fig. 3C). This result suggests that USP10 modulates TDP-43 expression at the post-transcriptional level. Regarding G3BP1 expression, USP10 overexpression did not have any effects on its transcript or protein levels (Fig. S3.F, G).

Although USP10 overexpression did not affect endogenous TDP-43 protein levels, this could be due to different homeostatic effects controlling its levels, such as auto-regulation. We thus decided to assess if USP10 might affect exogenous TDP-43 levels by co-transfecting USP10 with constructs expressing either GFP-TDP43-Wt or GFP-TDP43$^{\Delta NLS}$. Interestingly, co-transfection of either TDP-43 constructs with USP10 led to an obvious increase in the co-expression of GFP-TDP43 protein (Fig. 3D), an effect that was not seen at the mRNA level (Fig. S3A), suggesting again that USP10 may indeed control the stability of TDP-43 protein post-transcriptionally in different subcellular compartments. Remarkably, despite the further increase in GFP-TDP43$^{\Delta NLS}$ overexpression levels reached upon co-transfection with USP10 (Fig. 3D), TDP-43 cytoplasmic aggregation was still reduced (Fig. 1B, C).

In order to test whether this effect of USP10 on exogenous TDP-43 might be dependent on its deubiquitinase activity or its binding to G3BP1, we again used the USP10^{C424A} and USP10^{F10A} mutants in co-transfection experiments with GFP-TDP43$^{\Delta NLS}$ and analysed exogenous TDP-43 protein levels. First, we confirmed by immunoblot that all USP10 constructs were expressed at similar levels after co-transfection (Fig. S3B, C, D). Second, we quantified GFP-TDP43 protein levels by immunoblot, showing that all three USP10 constructs were able to increase exogenous TDP-43 levels at a similar degree when compared to the EV control (Fig. S3E). Thus, USP10 seems to control exogenous TDP-43 levels through a distinct mechanism that is not mediated by its deubiquitinase activity or by its ability to bind G3BP1.

Since the co-transfection experiments with USP10 and GFP-TDP43 showed a clearer effect than on endogenous TDP-43 levels, we also tried this approach in the context of USP10 downregulation. In this scenario, transfection of GFP-TDP43, both in its nuclear and cytoplasmic forms, in conditions where USP10 was previously downregulated via siRNA, led to highly reduced exogenous GFP-TDP43 levels when compared to the siRNA control (Fig. 3E), the opposite effects seen in conditions of USP10 overexpression (Fig. 3D). Overall, all these results suggest that USP10 positively regulates TDP-43 expression at the post-transcriptional level.

USP10 enhances TDP-43 functionality on splicing

Our results so far show that USP10 is able to modulate different aspects of TDP-43 biology including its aggregation and protein levels. Next, we tested whether this modulation also led to functional consequences at the mRNA splicing level. First, to test the effects of USP10 on TDP-43 functionality, we employed a widely used *CFTR* reporter minigene (Buratti & Baralle, 2001), cotransfecting the *CFTR* minigene together with USP10 in HeLa cells and assessing the percentage of exclusion (PSE) of *CFTR* exon 9. Our results show that USP10 overexpression is able to enhance endogenous TDP-43 splicing function when compared to the EV (Fig. 4A), without affecting TDP-43 protein or mRNA levels (Fig. 3A). We again used the two USP10 mutant constructs to mechanistically assess if this functional enhancement is mediated by USP10 deubiquitinase activity or by its interaction with G3BP1. Interestingly, both USP10 and USP10^{C424A} enhanced TDP-43 splicing function, although USP10^{F10A} did not (Fig. 4A).

In addition to the *CFTR* reporter minigene, we also assessed the PSE of endogenous exons known to be controlled by TDP-43 function, such as *RABGEF* exon 16 and *RGL* exon 2. In agreement with the minigene data, both USP10 and USP10^{C424A} overexpression caused an increase in TDP-43 splicing function on both targets when compared to the EV controls (Fig. 4B, C). However, the results with USP10^{F10A} were not as clear. Although for *RABGEF* it was clearly not different to the EV (Fig. 4B), in the case of *RGL*, USP10^{F10A} showed a clear tendency to behave as USP10 and USP10^{C424A} (Fig. 4C), suggesting that the F10A mutation might still lead to some enhanced TDP-43 splicing function. We obtained similar results in U2OS (Fig. S4A), demonstrating that, independently of the cell line and the splicing targets, USP10 is able to control the splicing functionality of endogenous TDP-43.

Next, we explored whether USP10 overexpression could also enhance TDP-43 splicing function in other contexts. First, we co-transfected the GFP-TDP43$^{\Delta NLS}$ (cytoplasmic) and GFP-TDP43 WT (nuclear) with USP10 in different cell lines, using the CFTR minigene and TDP-43 endogenous splicing targets as readouts for TDP-43 functionality. As expected, increasing TDP-43 levels with GFP-TDP43 WT transfection caused a strong increase in TDP-43 function on both the *CFTR* minigene and *RABGEF* exon 16 exclusion when compared to the EV. Remarkably, at least for the *CFTR* minigene, this increase in functionality was even further enhanced by co-transfection with USP10 (Fig. 4D, E). The increase in exogenous GFP-TDP43 protein levels that occurs upon co-transfection with USP10 (Fig. 3D) might contribute to this enhanced functionality. We then turned to the GFP-TDP43$^{\Delta NLS}$ construct, which on its own led to a decrease in TDP-43 splicing function when compared to the EV by reducing the PSE of *CFTR* exon 9 from the minigene, as it might affect endogenous TDP-43 functionality, perhaps through co-aggregation. In this model, USP10 co-transfection with the GFP-TDP43$^{\Delta NLS}$ construct led to an increase in the PSE for both, the *CFTR* minigene and *RABGEF* exon 16, when compared to the GFP-TDP43$^{\Delta NLS}$ transfection alone, thus enhancing TDP-43 splicing function, an effect that we could reproduce in different cell lines (Fig. S4A,B, C). Again, we tested the different USP10 mutant constructs on this setting, showing that while co-transfection of GFP-TDP43$^{\Delta NLS}$ with USP10^{C424A} rescued TDP-43 splicing function when compared to the GFP-TDP43$^{\Delta NLS}$ alone, USP10^{F10A} did not (Fig. 4F).

Finally, we tested whether USP10 would be able to rescue TDP-43 splicing function in other loss of function models. We turned to downregulation of *TARDBP* with siRNA in U2OS cells. As expected, we detected a strong decay in TDP-43 functionality in these conditions. USP10

overexpression in this TDP-43 loss of function model led to a small but significant increase in TDP-43 splicing function (Fig. 4G).

These set of results show that USP10 can positively modulate TDP-43 splicing function in different contexts, an effect that can occur without affecting endogenous TDP-43 expression levels (Fig. 3A) and is not mediated by USP10 enzymatic deubiquitinase activity.

USP10 affects alternative splicing overlapping with events controlled by TDP-43

Next, to assess for the first time the possible effects of USP10 on genome-wide alternative splicing, we turned into RNA-seq analysis in HeLa cells singly transfected with TDP-43, USP10, $USP10^{F10A}$ or $USP10^{C424A}$. First, we determined the splice junctions that were changed in each USP10 condition and compared them. Although there was a clear overlap between the three USP10 conditions, still the majority of the splicing events modified by each construct was unique for each of them (Fig. 5A). Next, we compared the splice junction events modified by overexpression of USP10 with those modified by TDP-43 overexpression also in Hela cells. Remarkably, this analysis revealed a clear overlap of the splicing junctions modified by USP10, $USP10^{F10A}$ and $USP10^{C424A}$ with a subset of those controlled by TDP-43 (Fig. 5B and S5A, B), with around 20% of the total splicing junctions modified after USP10 overexpression also moving in the same direction upon TDP-43 overexpression, leading to a positive correlation between the splicing events controlled by TDP-43 and those modified by USP10 and both mutants (Fig. 5C and S5C, D). Out of the 49 splice junction events changes shared between USP10 and TDP-43, around 50% were present in all three USP10 constructs (Fig. 5D). To visualize the differences and similarities between the splice junction events modified by TDP-43 overexpression and all USP10 constructs, we compared the percentage of splicing inclusion (PSI) of all the events shared upon TDP-43 and USP10 transfection and plotted them in comparison to USP10, $USP10^{F10A}$ and $USP10^{C424A}$ (Fig. 5E). Although overall, all three USP10 constructs shared the majority of splicing events that changed PSI upon USP10 overexpression, with independence of its catalytic activity or capacity to bind G3BP1, there were still some of junctions that were affected just by $USP10^{F10A}$, but not $USP10^{C424A}$ and viceversa. Altogether these results show for the first time that USP10 can modulate alternative splicing and that there is a correlation with some of the splicing events controlled by USP10 with a subset of those controlled by TDP-43.

As we showed that USP10 overexpression was able to enhance TDP-43 splicing function even under conditions of TDP-43 silencing (Fig. 4G), we turned onto an inducible shRNA model in HeLa cells to test the effects of USP10 overexpression under conditions of TDP-43 downregulation and quantify the effects on genome wide alternative splicing via RNA-seq analysis, focussing on the effects of USP10 on cryptic exon expression. Interestingly, USP10 was able to rescue a proportion (15%) of all the cryptic exons induced by TDP-43 downregulation, considering only the events that were modified by more than 10% upon USP10 overexpression when compared to EV. Figure 5F shows the cryptic exons which expression were most strongly reduced upon USP10 overexpression. To specifically assess the possible effects of USP10 on a prominent, disease related cryptic exon, we used a *UNC13A* minigene construct in TDP-43 silenced U2OS cells and co-transfected with USP10, showing that USP10 was able to rescue the expression of the *UNC13A* cryptic exon (Fig. S5E) (Brown

et al., 2022). Thus, USP10 is able to reduce the expression of at least of subset of TDP-43 dependent cryptic exons, counteracting some of the toxic effects of TDP-43 loss of function.

TDP-43 affects USP10 levels and function

Until now, we have shown that USP10 modulates different aspects of TDP-43 biology, including its aggregation, expression and splicing function. Next, we wondered whether a mutual, bidirectional modulation between the two proteins was occurring, whereby TDP-43, in turn, could control USP10 in a sort of feedback loop.

We began by modulating TDP-43 levels by either overexpression or downregulation in different cell lines and assessing possible effects on endogenous USP10 levels at the protein and transcript levels. TDP-43 overexpression did not affect endogenous USP10 levels in Hela cells (Fig. S6A, B) or U2OS (Fig. 6A). Given our previous results in co-expression experiments with TDP-43 and USP10, we assessed whether USP10 protein and transcript levels changed upon co-transfection with TDP-43. Indeed, total USP10 protein levels (that cannot distinguish between exogenous and endogenous USP10), were significantly lower when co-transfected together with TDP-43 compared to levels achieved by USP10 transfection alone (Fig. 6A).

In terms of downregulation, diminishing TDP-43 levels by siRNA in Hela or SH-SY5Y cells led to a significant reduction in endogenous USP10 protein (Fig. S6C and 6B), that was also reflected at the transcript level, and was also identified in the RNA-seq data from Hela cells with an inducible downregulation of *TARDBP* via shRNA (Fig. 6C). We also assessed USP10 levels when co-transfected together with siRNA against TDP-43. *USP10* transcript levels were significantly higher after co-transfection with USP10 and siRNA against TDP-43, when compared to the USP10 levels achieved after co-transfection with an siRNA against luciferase (Fig. 6D). Overall, these results suggest that TDP-43 controls USP10 levels.

As TDP-43 downregulation leads to reduced USP10 levels, we tested whether this would have functional consequences on the deubiquitinase activity of USP10. Thus, we assessed p53 levels as one of the main targets of USP10 deubiquitinase activity in an inducible SK-N-BE neuronal cell line expressing shRNA against *TARDBP* upon doxycycline treatment. As predicted, basal p53 levels were lower under conditions of TDP-43 downregulation when compared to untreated cells (Fig. 6E). This result suggests that TDP-43 control of USP10 might lead to functional consequences, linking to our knowledge for the first time the biologies of TDP-43 and p53.

To further explore the effects of TDP-43 loss of function on USP10, we turned into a cellular model with chronic TDP-43 loss of function. Immortalised mouse embryonic fibroblasts (MEFs) from *Tardbp*$^{F210I/F210I}$ KI mice carry a hypomorphic mutation in the second RNA binding domain of mouse TDP-43 that diminishes its RNA binding capacity without affecting TDP43 protein levels, leading to a profound but incomplete chronic loss of TDP-43 splicing function (Fratta et al., 2018). Interestingly, we found increased USP10 protein and transcript levels in *Tardbp*$^{F210I/F210I}$ MEFs when compared to controls (Fig. 6F, G). Overall, these data suggest that TDP-43 dysfunction leads to complex and dynamic changes in USP10 levels that might have functional consequences.

Finally, we tested whether TDP-43 overexpression and downregulation had an influence on USP10 subcellular localization and aggregation. In U2OS cells, transfection of TDP-43 WT, or TDP-43$^{\Delta NLS}$ led USP10 to aggregate in the cytoplasm, significantly increasing the

percentage of cells with USP10 inclusions and the number of USP10 inclusions per cell when compared with the EV control (Fig S6D). Moreover, the mean fluorescence ratio of nuclear to cytoplasmic USP10 decreased after TDP-43 overexpression (Fig S6D), suggesting a possible switch of USP10 from the nucleus to the cytoplasm upon TDP-43 upregulation. On the other hand, when we downregulated TDP-43 in U2OS cells with siRNA, the ratio of nuclear to cytoplasmic USP10 increased, supporting the idea that TDP-43 might be affecting USP10 subcellular localization (Fig S6E). Overall, these data suggest that TDP-43 might also modulate USP10 subcellular distribution and aggregation.

USP10 is affected in TDP-43 proteinopathies

As TDP-43 proteinopathies are defined at the pathological level by cytoplasmic TDP-43 inclusions, we proceeded to assess USP10 in patient post-mortem material. First, as we have shown that TDP-43 controls USP10 levels, we assessed USP10 protein levels by immunoblotting in lysates from the motor cortex of ALS patients, finding a significant increase in USP10 levels in patients versus controls (Fig. 7A). Next, we assessed USP10 levels in the frontal cortex from FTD patients that exhibited different types of TDP-43 pathology (FTLD-TDP), which are classified based on the morphology and location of TDP-43 inclusions in the affected cortical areas, and whether they occur in conjunction with ALS (Lashley et al., 2015) (Laferrière et al., 2019). Our results show that USP10 is generally upregulated in the cortex of FTD patients when compared to controls ($p<0.05$) (Fig. S7A), particularly in those with type B TDP-43 pathology (FTLD-TDP type B) ($p<0.01$) (Fig. 7B), that are characterised by the presence of TDP-43 positive neuronal cytoplasmic inclusions in all cortical layers in patients that can combine FTD with ALS.

At the neuropathological level, we performed immunohistochemistry with antibodies against USP10 and phosphorylated TDP-43 (pTDP-43) in paraffin-fixed post-mortem samples from the frontal cortex of FTD patients, separating them by the different types of TDP-43 pathology (Fig. 7C). In agreement with a previous finding from spinal cord of ALS patients (Takahashi et al., 2022), we did not find any co-localization between USP10 and pTDP-43 aggregates by immunofluorescence analysis, that nevertheless verified the presence of the characteristic pTDP-43 staining in all pathology subtypes. Interestingly, in the frontal cortex of FTLD-TDP type B patients, and to a lesser extent also in FTLD-TDP type A samples, we found increased cytoplasmic immunoreactivity of USP10 in some neurons showing characteristic USP10 staining (Fig. 7D). Thus, USP10 levels and subcellular localization is altered at least in the cortex of different TDP-43 proteinopathies.

DISCUSSION

TDP-43 cytoplasmic aggregation is the main pathological hallmark defining TDP-43 proteinopathies, but how these aggregates are formed and what drives TDP-43 nuclear clearance have not yet been determined. Here, we propose USP10 as a new player in TDP-43 proteinopathies, regulating TDP-43 aggregation and functionality.

We began to assess a possible role for USP10 in TDP-43 aggregation using different cellular models leading to varying degrees of colocalization between TDP-43 and SGs. Our data shows that USP10 is able to regulate TDP-43 cytoplasmic aggregation in a variety of different models irrespective of its colocalization with SGs, through a mechanism independent of USP10 deubiquitinase activity that is mediated by USP10 interaction with G3BP1 (Fig. 1-2). This is

compatible with previous reports proposing that TDP-43 colocalization with SGs can be context dependent (Dewey et al., 2012), and could occur independent of SGs colocalization (Gasset-Rosa et al., 2019).

Takahashi *et al*. have recently described that USP10 promotes the clearance of TDP-43 cytoplasmic aggregates and the formation of TDP-43 aggresomes in cells treated with the proteasome inhibitor MG-132 (Takahashi et al., 2022). Their results are in contrast with our data, as we did not detect any induction of TDP-43 aggregation mediated by USP10. The differences between both studies are likely explained by the different cellular models used, as in their study they mainly focussed on the role of USP10 on TDP-43 aggregation specifically under conditions of proteasome inhibition, which we do not assess here. Interestingly, in their study, they found a direct interaction between TDP-43 and USP10, which we have replicated (data not shown), that is mediated by TDP-43 RNA binding capacity and is likely to play a role in the wider functional connections between TDP-43 and USP10.

In terms of expression, we found that USP10 controls TDP-43 levels, with the downregulation of USP10 leading to a small but significant decrease in TDP-43 protein levels (Fig. 3B, C), a reduction that was not reflected at the *TARDBP* transcript level. Although our results show that USP10 overexpression did not change endogenous TDP-43 levels (Fig. 3A), we found a major increase in exogenous TDP-43 protein levels when USP10 was cotransfected (Fig. 3D). Mechanistically, this increase in transfected TDP-43 protein levels upon USP10 cotransfection was, again, not reflected at the transcript level (Fig. S3A), and was not mediated by either USP10 deubiquitinase activity or by its interaction with G3BP1 (Fig. S3B-E). Overall, these results suggest that USP10 might control TDP-43 levels through a mechanism acting at the post-transcriptional level distinct to its actions on aggregation, since neither its deubiquitinase activity or binding to G3BP1 are required here.

We then focussed on the effects of USP10 on TDP-43 splicing function. We began by assessing the well known CFTR exon 9 reporter minigene system, as well as the inclusion of endogenous cassette exons known to be modulated by TDP-43 splicing function. Interestingly, we found that USP10 can indeed enhance endogenous TDP-43 splicing function in different cellular models through a mechanism that is not mediated by changes in endogenous TDP-43 protein levels. Further analysis via RNA-seq data revealed that USP10 overexpression leads to genome-wide alternative splicing alterations. Remarkably, around 20% of the alternative splicing events controlled by USP10 are also modulated in the same direction by TDP-43, highlighting the very close relation between the functions of both proteins. Mechanistically, overexpression of both $USP10^{F10A}$ and $USP10^{C424A}$ led to changes in alternative splicing, with a clear overlap in their splicing targets, but also with some unique changes for each mutation. Critically, USP10 overexpression was also capable of reducing the expression of around 20% of cryptic exons expressed in our inducible TDP-43 downregulation cellular model, without affecting the expression of *TARDBP*, suggesting that USP10 upregulation might be beneficial by counteracting at least some of the possible toxic effects of cryptic exon expression.

Having established that USP10 can control TDP-43 aggregation and functionality, we assessed whether TDP-43 could in turn affect USP10. Indeed, TDP-43 downregulation reduced USP10 transcript and protein levels confirmed by immunoblot, RT-PCR and RNA-seq (Fig. 5C, D, E), leading at least to functional effects affecting the levels of its downstream deubiquitinase target p53 (Fig. 5F), a critical tumour suppressor in cancer and guardian of the genome that has also

been recently found to be important in ALS (Maor-Nof et al., 2021). Furthermore, the control of USP10 by TDP-43 adds another layer of complexity to the role of TDP-43 in modulating stress granules formation beyond controlling the expression of other key SGs proteins such as G3BP1 and TIA1 (McDonald et al., 2011) (Sidibe, H, 2020).

We went on to establish whether USP10 was affected in ALS/FTD patient material. In post-mortem samples of cerebral cortex from ALS and FTLD-TDP patients, we observed that USP10 levels were significantly increased when compared to controls, particularly in the frontal cortex of FTLD-TDP type B patients (Fig. 6A, B). Interestingly, we also observed increased USP10 levels in MEFs derived from KI mice carrying a TDP-43 F210I hypomorphic mutation (Fig. 5G, H). These results are in clear contrast with the decrease in USP10 levels that we report in cellular models of acute TDP-43 downregulation (Fig. 5.C-E), which could indicate that the increase in USP10 levels seen in patients might be an effect of chronic loss of TDP-43 function, but further investigation will be clearly required to clarify this issue. Indeed, several studies have reported increased levels of USP10 in some types of cancer including glioblastoma (Grunda et al., 2006), as well as in affected neurons in PD (Takahashi et al., 2018). Interestingly, very recently, USP10 protein levels have been found to be inversely correlated with TDP-43 pathological burden in postmortem human motor neurons (Guise et al., 2024). Altogether, these results clearly show that USP10 is affected in TDP-43 proteinopathies.

Finally, at the pathological level, we found increased cytoplasmic immunoreactivity of USP10 in some neurons from the frontal cortex of FTLD-TDP patients, particularly in those with type B TDP-43 pathology (Fig. 6C), correlating with the upregulation of USP10 protein levels that did not colocalize with pathological TDP-43 inclusions in the cortex of FTLD-TDP patients (Fig. 6C), a finding compatible with previous data showing that pathological TDP-43 inclusions also did not colocalize with USP10 in spinal cord from ALS patients (Takahashi et al., 2022). Previously, USP10 has been found to colocalize with TAU positive inclusions in cortex from AD patients (Piatnitskaia et al., 2019), and also in Lewy bodies from Parkinson's disease patients (Takahashi et al., 2018). Thus, USP10 is altered in different neurodegenerative conditions, perhaps reflecting a previously proposed role for SGs as precursors of pathological aggregation in these conditions (Wolozin & Ivanov, 2019).

In conclusion, we describe a new functional interaction between USP10 and TDP-43, with both proteins affecting different aspects of the biology of the other. Indeed, our data suggest that USP10 controls the aggregation, expression and functionality of TDP-43, providing insights into some of the potential molecular mechanisms involved. In turn, our data also suggested that TDP-43 might be able to control USP10 protein levels, that we show might be altered in ALS and FTD, suggesting a possible involvement of USP10 in TDP-43 proteinopathies pathogenesis, giving potential clinical relevance to this new functional interaction between TDP-43 and USP10.

MATERIALS AND METHODS

Cell lines and cultures

All cell lines were cultured at 37º C with 5% CO_2. HeLa, U2OS, Neuro2a and MEFs (Fratta et al., 2018) were grown in DMEM media (31966, Gibco), whereas SH-SY5Y and SK-N-BE were grown in DMEM/F-12 (50:50), all supplemented with 10% FBS (10082147, Invitrogen) and 1% penicillin/streptomycin (10378016, Invitrogen).

The clover-TDP43$^{\Delta NLS}$ cell line was a gift from Don Cleveland (Gasset-Rosa et al., 2019). The inducible SK-N-BE cell line carrying a doxycycline inducible shRNA against TDP-43 have been already published (Brown et al., 2022). For the induction of *TARDBP* gene silencing, doxycycline (1 µg/ml) (D9891, Sigma) was administered in the culture medium for 3-6 days, depending on the experiment. The inducible Hela cell line carrying the doxycycline inducible shRNA against TDP-43 were generated from a HeLa ATCC clone (CCL-2). Briefly, cells were transduced with an inducible system Tet-pLKO-puro (21915, Addgene) encoding an shRNA targeting *TARDBP* sequence (TRCN0000016038, SIGMA). Lentiviral particles were produced in the HEK293T cell line using psPAX2 (12260, Addgene) and pMD2.G (12259, Addgene) plasmids (both a gift from Dr. Trono). HeLa cells were transduced and selected with puromycin (1 µg/ml) for two weeks. A single clone was isolated and tested the KD efficiency (>80% reduction in protein expression) by doxycycline (200 ng/µl) exposure for three days.

Transfections were performed with either jetPRIME (101000046, Polyplus), Lipofectamine 3000 (L3000015, Thermo Fisher) or electroporation with an Amaxa Nucleofector 2b device (AAB-1001, Lonza), all following manufacturer instructions. For all co-transfections experiments, the same amount of DNA for each construct and total DNA was used in all conditions, including the single transfections. Cells were transfected and collected after 24 hours, unless otherwise stated.

Cellular stress treatments. To induce TDP-43 cytoplasmic localization and SGs in SH-SY5Y, coverslip- plated cells were treated with 500 µM sodium arsenite for 40 minutes, followed by incubation with 600 mM sorbitol for 40 minutes. Cells were then left to recover with fresh media for 1 hour and coverslips processed for microscopy. To induce SGs in U2OS cells, 250 µM sodium arsenite was used for 80 minutes. To induce TDP-43 cytoplasmic aggregates in the clover-TDP43$^{\Delta NLS}$ cell line, TDP-43 cytoplasmic localization was induced by doxycycline treatment (1 µg/ml doxycyclin for 24 hours), followed by 250 µM sodium arsenite for 80 minutes. To induce the formation of stress granules and aggregation of TDP-43 in the nucleus, USOS or HeLa cells were treated with 500 µM sodium arsenite for 30 minutes.

Small interfering RNAs (siRNAs) specific to human TDP-43 (siTDP43: GCAAAGCCAAGAUGAGCCUTTdTdT), human USP10 (siUSP10.2: CCCUGAUGGUAUCACUAAAGAdTdT) or negative control luciferase (siLuc: CGUACGCGGAAUACUUCGAUU dTdT), were transfected into U2OS or HeLa cells using Lipofectamine RNAiMAX reagents (Invitrogen) according to the manufacturer's protocol. When a combination of downregulation and overexpression was performed a first round of downregulation was performed on day, followed by a second round on day 2. Then, on day 3, cells were transfected for overexpression using lipofectamine 3000, and harvested on the next day.

Constructs

The GFP-tagged TDP-43-WT and TDP-43$^{\Delta NLS}$ constructs were a gift from the laboratory of Leonard Petrucelli (Wang et al., 2013). The CFTR C155T TG11T5 minigene was a gift from

Emanuele Buratti (Pagani et al., 2003) (D'Ambrogio et al., 2009). The USP10 WT and $USP10^{C424A}$ construct were developed by the group of Lorenza Penengo (University of Zurich, Switzerland). The $USP10^{F10A}$ mutant was made using site directed mutagenesis following manufacturer instructions (Agilent). All constructs were amplified in commercial *E. coli* lines and plasmids purified (740410.50, Macherey Nagel) according to the manufacturer's instructions.

Antibodies

The following antibodies and concentrations were used for immunoblot and immunofluorescence staining:

Rabbit anti TDP-43 (WB 1:1000, IF 1:400, Protein Tech, 10782-2-AP); mouse anti TDP-43 (WB 1:5000, abcam, ab104223); mouse anti TDP-43 (IF 1:200, R&D systems, MAB37778); mouse anti pTDP-43 (IF 1:3000, Cosmobio, CAC-TIP-PTD-M01); mouse anti G3BP1 (IF 1:300, Protein Tech, 66486-1-Ig); rabbit anti G3BP1 (WB: 1:2000, IF 1:300, Protein Tech, 13057-2-AP); rabbit anti G3BP2 (IF 1:300, Protein Tech, 16276-1-AP); rabbit anti USP10 (WB 1:1000, IF 1:500, Sigma-Aldrich, HPA006731); rabbit anti USP10 (WB 1:1000, made in house from the Freire laboratory); rabbit anti USP10 (IF 1:200, Bethyl, A300-901A); mouse anti p53 (WB 1:500, Santa Cruz Biotechnology, sc-126); mouse anti Tubulin (WB 1:10000, Protein Tech, 11224-1-AP); mouse anti β-Tubulin (WB 1:10000, Protein Tech, 66240-1-Ig); mouse anti GAPDH (WB 1:250, Santa Cruz Biotechnology, sc-32233); anti mouse Alexa Fluor 488 (IF secondary 1:600, Thermo Fisher, Z25002); anti rabbit Alexa Fluor 488 (IF secondary 1:600, Thermo Fisher, Z25302); anti mouse Alexa Fluor 568 (IF secondary 1:600, Thermo Fisher, Z25006); anti rabbit Alexa Fluor 568 (IF secondary 1:600, Thermo Fisher, Z25306).

Patient material

We obtained frontal cortex brain tissue from the Brain Bank of the University College of London, separated according to the subtype of TDP-43 pathology and a control group of deceased patients with no pathologies described. Lysates from ALS motor cortex and controls came from the Bellvitge Hospital (Barcelona). All biological samples comply with the legal requirements of consent, collection, use and storage.

Immunofluorescence

Cells were grown in plates containing sterile glass coverslips, fixed with 4 % PFA (P6148, Sigma-Aldrich), permeabilised using 0.5% Triton detergent (85111, Thermo Fisher) and blocked with BSA (422381B, VWR). The samples were then incubated overnight with primary antibodies in BSA, and then with appropriate secondary antibodies. Slides were mounted using ProLong™ (P36962, Thermo Fisher) and samples visualised on a Zeiss Axio Observer fluorescence microscope, with images analysed using Image J software (Schneider et al., 2012).

The *immunohistochemistry* experiments from patient material were carried out on 20 μm thick paraffin-embedded sections obtained from the Queen Square Brain Bank for Neurological Disorders (University College of London). Antigenic unmasking was performed using the Dako PT Link PT100 Slide Stainer (Swerdlick Medical Systems), prior to permeabilization with 0.5% Triton. Immunofluorescence or DAB was used for visualized (15454629, Thermo Fisher) using a Leica DMi1 light microscope.

For the detection and quantification of TDP-43-positive aggregates and SGSs, pictures of 50-100 cells from random fields were taken with a Zeiss Axio Observer fluorescence microscope, and the images taken analysed using Image J software. Aggregates were analyzed with the Stress Granules Counter or the Aggrecount Image J plugins. The data collected were the

number of aggregates per cell, the number of cells with aggregates and the size of the aggregates. To consider that a cell had TDP-43 inclusions or SG, cells with more than 2 inclusions/SG larger than 0.5-1 μm^2 were taken as positive. For colocalization studies, a line profile analysis was performed and the quantification was done using JaCoP in Image J giving the Pearson coefficient and the mass centre coincidence (Bolte & Cordelières, 2006). To determine the intensity of TDP-43 or USP10 fluorescence, either the nucleus or the cytoplasm were selected in each cell and the mean of fluorescence was directly assessed in Image J, with 40-60 cells processed.

Protein extractions

From cell lines, proteins were extracted by resuspending cells from 6-well plates in 100 µl of RIPA or 7M Urea Buffer containing protease inhibitor (11873580001, Roche) and, if necessary, phosphatase inhibitor (04906837001, Roche). Cell lysates were centrifuged at >14 000 x g for 15 minutes, discarding the sediment. Supernatant was then sonicated using an ultrasonic homogeniser (UP50H, Hielscher) for 15 seconds. Protein concentration in the soluble extract was quantified by using the BCA method (Thermo Scientific). For post-mortem material from FTD patients, 13mg of frozen sample was weighed, to which 0.26 ml of 7M Urea buffer was added and homogenised using a rotary homogeniser (BK-HG, Biobase). The samples were then sonicated using an ultrasonic homogeniser (UP50H, Hielscher) for 15 seconds. Samples were frozen at -80°C until use.

Immunoblots

Cell lysates were resuspended in Laemmli buffer and heated at 95°C during 5 minutes. Then, proteins were separated by 10% SDS polyacrylamide gel electrophoresis (SDS-PAGE) using a Mini-PROTEAN kit (1658001FC, Bio-Rad). Between 20 and 50 µg of protein per well were loaded. After the separation, proteins were transferred onto a nitrocellulose (1620115, BioRad) or PVDF (1620177, Bio-Rad) membrane, that was blocked with either BSA or milk powder. The primary antibodies and concentrations used are listed in the antibodies section. Bands were detected via ECL (1705060, Bio-Rad), viewed on a ImageQuant™ LAS 4000 chemiluminescence reader (GE Healthcare), and analysed by densitometry using the Image Quant TL software.

RNA isolation, RT–PCR and qPCR

RNA extractions were carried out using TRIzol (15596-026, Invitrogen), according to manufacturer instructions. For complementary DNA synthesis, the qScript cDNA synthesis kit (95047, QuantaBio) was used, using as a template 100-500 ng of RNA. RT-PCR for splicing events was conducted using 2X PCR Master Mix (11816843, Thermo Fisher) with specific primers (see below) spanning the differentially expressed exon. Products were electrophoresed on 2.5% agarose gels containing ethidium bromide, and visualized on an automated image detection system (Gel Doc EZ, BioRad). The BioRad Image Lab software was used to quantify the bands. Results were analysed using the percentage of exclusion (PSE), calculated dividing the intensity of the shorter exon exclusion band by the sum of both exon inclusion and exon exclusion bands. Primers used here were:

RABGEF exon 16: CTGCAGACAAAGCACACACGAT and GCACAGAGGAGATCCGATTGAT

RGL exon 2: GACGGAGTCGAAAGGTCAAA and CCACAGGTTTCACCTCCATC

CFTR minigene: CAACTTCAAGCTCCTAAGCCACTGC and TAGGATCCGGTCACCAGGAAGTTGGTTAAATCA
UNC13A minigene: TCCTCACTCTCTCTGACGAGG and CATGGCGGCGGTCGACCTAG

qPCR was used to quantify mRNA expression using specific primers (see below). SYBR Green (PB20.11-05, PCR Biosystems) was used on a real-time thermal cycler (LightCycler® 480, Roche). *S16* or *HPRT* were used as internal control gene. The levels of messenger RNA were assessed by calculating ΔΔCT which shows the relative expression change (fold change), normalised to the housekeeping gene. For all samples analysed, 3 technical replicates and 3 biological replicates were performed. The primers:
GFP: AAGCAGAAGAACGGCATCAAG and TCAGGTAGTGGTTGTCGGGCA
Human *USP10*: GGGTGCCAGAAGCTTATCAA and CACTGTTGCCGTGATGGTAG
Mouse *Usp10*: TGCCTTTGAACCCACATACA and TCAGGCTCAGCATCTCTCTTCA
Human *TARDBP (exon 1-2)*: CTGCTTCGGTGTCCCTGT and ATGGGCTCATCGTTCTCATC
Human *TARDBP (exon 5-6)*: ATGACTGAGGATGAGCTGCG and CACAAAGAGACTGCGCAATCT
Human *S16*: AAGTCTTCGGACGCAAGAAA and TGCCCAGAAGCAGAACAG
Mouse *S16*: TTCTGGGCAAGGAGCGATT and GATGGACTGTCGGATGGCA
Human *HPRT*: TTTGCTGACCTGCTGCTGGATTAC and TTGACCATCTTTGGATTATACTGC

RNA sequencing analysis

Raw sequences (in fastq format) were trimmed using Fastp109 with the parameter "qualified_quality_phred: 10", and aligned using STAR (v2.7.0f)110 to the Grch38 with gene models from GENCODE v40.111 (Chen et al., 2018) (Dobin et al., 2013).
The STAR outputs are BAM files, containing the counts and coordinates for all splice junctions found in the sample, and alignment metadata including the genomic location where a read is mapped to, read sequence, and quality score. Then, using samtools112, BAM files were sorted and indexed by the read coordinates location (Li et al., 2009).
Trimmed fastqc files were aligned to the transcriptome using Salmon (v1.5.1)113, outputting isoform-specific counts used for differential gene expression, performed using DeSEQ2114 without covariates, using an index built from GENCODE v40.111 (Patro et al., 2017) (Love et al., 2014) (Frankish et al., 2019). The DESeq2 median of ratios, which controls for both sequencing depth and RNA composition, was used to normalise gene counts. Differential expression was defined at a Benjamini–Hochberg false discovery rate < 0.1. We kept genes with at least 5 counts per million in more than 2 samples.
Splicing analysis was performed using Majiq (v2.1)115 on STAR-aligned and sorted BAMs and the Grch38 reference genomes. MAJIQ's outputs were used to categorise each of the splicing junctions by the overlap with annotated transcripts and exons, using GTF and DASPER (https://github.com/dzhang32/dasper), classifying them into "annotated", "novel_acceptor", "novel_donor", "novel_exon_skip", "novel_combo" and "ambig_gene" and "none" (Vaquero-Garcia et al., n.d.). Cryptic splicing was defined as junctions with Ψ (PSI, percent spliced in) < 5% the in control samples, ΔΨ > 10% between groups, and the junction were unannotated in GENCODE v40.111 In some cases for a cryptic exon, there was only enough coverage to call one of the two defining junctions significant.

The alignment and splicing pipelines are implemented in Snakemake (v5.5.4)116, a workflow management software that allows reliable, reproducible, and scalable analysis, and run on the UCL high-performance cluster (HPC) (Mölder et al., 2021). DESeq2 and data visualisation were run on R using custom scripts available upon request.

Statistics

Results were analysed using GraphPad Prism 8.0.2 software. Data are generally presented as the mean accompanied by the standard error (Mean±SEM). Test and sample sizes used are generally specified in each figure. For parametric samples, t-test and/or ANOVA was performed. For non-parametric samples, the Mann-Whitney U test was used. Statistical significance is attributed at a p value <0.05.

Acknowledgements

REFERENCES

Advani, V. M., & Ivanov, P. (2020). Stress granule subtypes: An emerging link to neurodegeneration. *Cellular and Molecular Life Sciences*, *77*(23), 4827–4845. https://doi.org/10.1007/s00018-020-03565-0

Aulas, A., Stabile, S., & Vande Velde, C. (2012). Endogenous TDP-43, but not FUS, contributes to stress granule assembly via G3BP. *Molecular Neurodegeneration*, *7*(1), 1. https://doi.org/10.1186/1750-1326-7-54

Aulas, A., & Vande Velde, C. (2015). Alterations in stress granule dynamics driven by TDP-43 and FUS: A link to pathological inclusions in ALS? *Frontiers in Cellular Neuroscience*, *9*. https://doi.org/10.3389/fncel.2015.00423

Bolte, S., & Cordelières, F. P. (2006). A guided tour into subcellular colocalization analysis in light microscopy. *Journal of Microscopy*, *224*(3), 213–232. https://doi.org/10.1111/j.1365-2818.2006.01706.x

Bomberger, J. M., Barnaby, R. L., & Stanton, B. A. (2009). The Deubiquitinating Enzyme USP10 Regulates the Post-endocytic Sorting of Cystic Fibrosis Transmembrane Conductance Regulator in Airway Epithelial Cells. *Journal of Biological Chemistry*, *284*(28), 18778–18789. https://doi.org/10.1074/jbc.M109.001685

Brown, A.-L., Wilkins, O. G., Keuss, M. J., Hill, S. E., Zanovello, M., Lee, W. C., Bampton, A., Lee, F. C. Y., Masino, L., Qi, Y. A., Bryce-Smith, S., Gatt, A., Hallegger, M., Fagegaltier, D., Phatnani, H., NYGC ALS Consortium, Phatnani, H., Kwan, J., Sareen, D., … Fratta, P. (2022). TDP-43 loss and ALS-risk SNPs drive mis-splicing and depletion of UNC13A. *Nature*, *603*(7899), 131–137. https://doi.org/10.1038/s41586-022-04436-3

Buratti, E. (2021). Trends in Understanding the Pathological Roles of TDP-43 and FUS Proteins. In B. Ghetti, E. Buratti, B. Boeve, & R. Rademakers (Eds.), *Frontotemporal Dementias* (Vol. 1281, pp. 243–267). Springer International Publishing. https://doi.org/10.1007/978-3-030-51140-1_15

Buratti, E., & Baralle, F. E. (2001). Characterization and Functional Implications of the RNA Binding Properties of Nuclear Factor TDP-43, a Novel Splicing Regulator of CFTR Exon 9. *Journal of Biological Chemistry*, *276*(39), 36337–36343. https://doi.org/10.1074/jbc.M104236200

Chen, S., Zhou, Y., Chen, Y., & Gu, J. (2018). fastp: An ultra-fast all-in-one FASTQ preprocessor. *Bioinformatics*, *34*(17), i884–i890. https://doi.org/10.1093/bioinformatics/bty560

Clague, M. J., Barsukov, I., Coulson, J. M., Liu, H., Rigden, D. J., & Urbé, S. (2013). Deubiquitylases From Genes to Organism. *Physiological Reviews*, *93*(3), 1289–1315. https://doi.org/10.1152/physrev.00002.2013

Cook, C., & Petrucelli, L. (2019). Genetic Convergence Brings Clarity to the Enigmatic Red Line in ALS. *Neuron*, *101*(6), 1057–1069. https://doi.org/10.1016/j.neuron.2019.02.032

Coyne, A. N., Zaepfel, B. L., & Zarnescu, D. C. (2017). Failure to Deliver and Translate—New Insights into RNA Dysregulation in ALS. *Frontiers in Cellular Neuroscience*, *11*, 243. https://doi.org/10.3389/fncel.2017.00243

D'Ambrogio, A., Buratti, E., Stuani, C., Guarnaccia, C., Romano, M., Ayala, Y. M., & Baralle, F. E. (2009). Functional mapping of the interaction between TDP-43 and hnRNP A2 in vivo. *Nucleic Acids Research*, *37*(12), 4116–4126. https://doi.org/10.1093/nar/gkp342

Dewey, C. M., Cenik, B., Sephton, C. F., Johnson, B. A., Herz, J., & Yu, G. (2012). TDP-43 aggregation in neurodegeneration: Are stress granules the key? *Brain Research*, *1462*, 16–25. https://doi.org/10.1016/j.brainres.2012.02.032

Dobin, A., Davis, C. A., Schlesinger, F., Drenkow, J., Zaleski, C., Jha, S., Batut, P., Chaisson, M., & Gingeras, T. R. (2013). STAR: Ultrafast universal RNA-seq aligner. *Bioinformatics*, *29*(1), 15–21. https://doi.org/10.1093/bioinformatics/bts635

Ederle, H., & Dormann, D. (2017). TDP -43 and FUS *en route* from the nucleus to the cytoplasm. *FEBS Letters*, *591*(11), 1489–1507. https://doi.org/10.1002/1873-3468.12646

Fang, M. Y., Markmiller, S., Vu, A. Q., Javaherian, A., Dowdle, W. E., Jolivet, P., Bushway, P. J., Castello, N. A., Baral, A., Chan, M. Y., Linsley, J. W., Linsley, D., Mercola, M., Finkbeiner, S., Lecuyer, E., Lewcock, J. W., & Yeo, G. W. (2019). Small-Molecule Modulation of TDP-43 Recruitment to Stress Granules Prevents Persistent TDP-43 Accumulation in ALS/FTD. *Neuron*, *103*(5), 802-819.e11. https://doi.org/10.1016/j.neuron.2019.05.048

Frankish, A., Diekhans, M., Ferreira, A.-M., Johnson, R., Jungreis, I., Loveland, J., Mudge, J. M., Sisu, C., Wright, J., Armstrong, J., Barnes, I., Berry, A., Bignell, A., Carbonell Sala, S., Chrast, J., Cunningham, F., Di Domenico, T., Donaldson, S., Fiddes, I. T., … Flicek, P. (2019). GENCODE reference annotation for the human and mouse genomes. *Nucleic Acids Research*, *47*(D1), D766–D773. https://doi.org/10.1093/nar/gky955

Fratta, P., Sivakumar, P., Humphrey, J., Lo, K., Ricketts, T., Oliveira, H., Brito-Armas, J. M., Kalmar, B., Ule, A., Yu, Y., Birsa, N., Bodo, C., Collins, T., Conicella, A. E., Mejia Maza, A., Marrero-Gagliardi, A., Stewart, M., Mianne, J., Corrochano, S., … Acevedo-Arozena, A. (2018). Mice with endogenous TDP -

43 mutations exhibit gain of splicing function and characteristics of amyotrophic lateral sclerosis. *The EMBO Journal*, *37*(11). https://doi.org/10.15252/embj.201798684

Gasset-Rosa, F., Lu, S., Yu, H., Chen, C., Melamed, Z., Guo, L., Shorter, J., Da Cruz, S., & Cleveland, D. W. (2019). Cytoplasmic TDP-43 De-mixing Independent of Stress Granules Drives Inhibition of Nuclear Import, Loss of Nuclear TDP-43, and Cell Death. *Neuron*, *102*(2), 339-357.e7. https://doi.org/10.1016/j.neuron.2019.02.038

Grunda, J. M., Nabors, L. B., Palmer, C. A., Chhieng, D. C., Steg, A., Mikkelsen, T., Diasio, R. B., Zhang, K., Allison, D., Grizzle, W. E., Wang, W., Gillespie, G. Y., & Johnson, M. R. (2006). Increased Expression of Thymidylate Synthetase (TS), Ubiquitin Specific Protease 10 (USP10) and Survivin is Associated with Poor Survival in Glioblastoma Multiforme (GBM). *Journal of Neuro-Oncology*, *80*(3), 261–274. https://doi.org/10.1007/s11060-006-9191-4

Guise, A. J., Misal, S. A., Carson, R., Chu, J.-H., Boekweg, H., Van Der Watt, D., Welsh, N. C., Truong, T., Liang, Y., Xu, S., Benedetto, G., Gagnon, J., Payne, S. H., Plowey, E. D., & Kelly, R. T. (2024). TDP-43-stratified single-cell proteomics of postmortem human spinal motor neurons reveals protein dynamics in amyotrophic lateral sclerosis. *Cell Reports*, *43*(1), 113636. https://doi.org/10.1016/j.celrep.2023.113636

He, Y., Jiang, S., Mao, C., Zheng, H., Cao, B., Zhang, Z., Zhao, J., Zeng, Y., & Mao, X. (2021). The deubiquitinase USP10 restores PTEN activity and inhibits non–small cell lung cancer cell proliferation. *Journal of Biological Chemistry*, *297*(3), 101088. https://doi.org/10.1016/j.jbc.2021.101088

Hofmann, S., Kedersha, N., Anderson, P., & Ivanov, P. (2021). Molecular mechanisms of stress granule assembly and disassembly. *Biochimica et Biophysica Acta (BBA) - Molecular Cell Research*, *1868*(1), 118876. https://doi.org/10.1016/j.bbamcr.2020.118876

Ivanov, P., Kedersha, N., & Anderson, P. (2019). Stress Granules and Processing Bodies in Translational Control. *Cold Spring Harbor Perspectives in Biology*, *11*(5), a032813. https://doi.org/10.1101/cshperspect.a032813

Kedersha, N., Panas, M. D., Achorn, C. A., Lyons, S., Tisdale, S., Hickman, T., Thomas, M., Lieberman, J., McInerney, G. M., Ivanov, P., & Anderson, P. (2016). G3BP–Caprin1–USP10 complexes mediate stress granule condensation and associate with 40S subunits. *Journal of Cell Biology*, *212*(7), e201508028. https://doi.org/10.1083/jcb.201508028

Laferrière, F., Maniecka, Z., Pérez-Berlanga, M., Hruska-Plochan, M., Gilhespy, L., Hock, E.-M., Wagner, U., Afroz, T., Boersema, P. J., Barmettler, G., Foti, S. C., Asi, Y. T., Isaacs, A. M., Al-Amoudi, A., Lewis, A., Stahlberg, H., Ravits, J., De Giorgi, F., Ichas, F., … Polymenidou, M. (2019). TDP-43 extracted from frontotemporal lobar degeneration subject brains displays distinct aggregate assemblies and neurotoxic effects reflecting disease progression rates. *Nature Neuroscience*, *22*(1), 65–77. https://doi.org/10.1038/s41593-018-0294-y

Lashley, T., Rohrer, J. D., Mead, S., & Revesz, T. (2015). Review: An update on clinical, genetic and pathological aspects of frontotemporal lobar degenerations. *Neuropathology and Applied Neurobiology*, *41*(7), 858–881. https://doi.org/10.1111/nan.12250

Lee, K.-H., Zhang, P., Kim, H. J., Mitrea, D. M., Sarkar, M., Freibaum, B. D., Cika, J., Coughlin, M., Messing, J., Molliex, A., Maxwell, B. A., Kim, N. C., Temirov, J., Moore, J., Kolaitis, R.-M., Shaw, T. I., Bai, B., Peng, J., Kriwacki, R. W., & Taylor, J. P. (2016). C9orf72 Dipeptide Repeats Impair the Assembly,

Dynamics, and Function of Membrane-Less Organelles. *Cell*, *167*(3), 774-788.e17. https://doi.org/10.1016/j.cell.2016.10.002

Lee, Y.-B., Scotter, E. L., Lee, D.-Y., Troakes, C., Mitchell, J., Rogelj, B., Gallo, J.-M., & Shaw, C. E. (2021). Cytoplasmic TDP-43 is involved in cell fate during stress recovery. *Human Molecular Genetics*, *31*(2), 166–175. https://doi.org/10.1093/hmg/ddab227

Li, H., Handsaker, B., Wysoker, A., Fennell, T., Ruan, J., Homer, N., Marth, G., Abecasis, G., Durbin, R., & 1000 Genome Project Data Processing Subgroup. (2009). The Sequence Alignment/Map format and SAMtools. *Bioinformatics*, *25*(16), 2078–2079. https://doi.org/10.1093/bioinformatics/btp352

Ling, S.-C., Polymenidou, M., & Cleveland, D. W. (2013). Converging Mechanisms in ALS and FTD: Disrupted RNA and Protein Homeostasis. *Neuron*, *79*(3), 416–438. https://doi.org/10.1016/j.neuron.2013.07.033

Liu, J., Xia, H., Kim, M., Xu, L., Li, Y., Zhang, L., Cai, Y., Norberg, H. V., Zhang, T., Furuya, T., Jin, M., Zhu, Z., Wang, H., Yu, J., Li, Y., Hao, Y., Choi, A., Ke, H., Ma, D., & Yuan, J. (2011). Beclin1 Controls the Levels of p53 by Regulating the Deubiquitination Activity of USP10 and USP13. *Cell*, *147*(1), 223–234. https://doi.org/10.1016/j.cell.2011.08.037

Love, M. I., Huber, W., & Anders, S. (2014). Moderated estimation of fold change and dispersion for RNA-seq data with DESeq2. *Genome Biology*, *15*(12), 550. https://doi.org/10.1186/s13059-014-0550-8

Maor-Nof, M., Shipony, Z., Lopez-Gonzalez, R., Nakayama, L., Zhang, Y.-J., Couthouis, J., Blum, J. A., Castruita, P. A., Linares, G. R., Ruan, K., Ramaswami, G., Simon, D. J., Nof, A., Santana, M., Han, K., Sinnott-Armstrong, N., Bassik, M. C., Geschwind, D. H., Tessier-Lavigne, M., … Gitler, A. D. (2021). P53 is a central regulator driving neurodegeneration caused by C9orf72 poly(PR). *Cell*, *184*(3), 689-708.e20. https://doi.org/10.1016/j.cell.2020.12.025

Markmiller, S., Soltanieh, S., Server, K. L., Mak, R., Jin, W., Fang, M. Y., Luo, E.-C., Krach, F., Yang, D., Sen, A., Fulzele, A., Wozniak, J. M., Gonzalez, D. J., Kankel, M. W., Gao, F.-B., Bennett, E. J., Lécuyer, E., & Yeo, G. W. (2018). Context-Dependent and Disease-Specific Diversity in Protein Interactions within Stress Granules. *Cell*, *172*(3), 590-604.e13. https://doi.org/10.1016/j.cell.2017.12.032

McDonald, K. K., Aulas, A., Destroismaisons, L., Pickles, S., Beleac, E., Camu, W., Rouleau, G. A., & Vande Velde, C. (2011). TAR DNA-binding protein 43 (TDP-43) regulates stress granule dynamics via differential regulation of G3BP and TIA-1. *Human Molecular Genetics*, *20*(7), 1400–1410. https://doi.org/10.1093/hmg/ddr021

Mehta, P. R., Brown, A.-L., Ward, M. E., & Fratta, P. (2023). The era of cryptic exons: Implications for ALS-FTD. *Molecular Neurodegeneration*, *18*(1), 16. https://doi.org/10.1186/s13024-023-00608-5

Mölder, F., Jablonski, K. P., Letcher, B., Hall, M. B., Tomkins-Tinch, C. H., Sochat, V., Forster, J., Lee, S., Twardziok, S. O., Kanitz, A., Wilm, A., Holtgrewe, M., Rahmann, S., Nahnsen, S., & Köster, J. (2021). Sustainable data analysis with Snakemake. *F1000Research*, *10*, 33. https://doi.org/10.12688/f1000research.29032.2

Neumann, M., Sampathu, D. M., Kwong, L. K., Truax, A. C., Micsenyi, M. C., Chou, T. T., Bruce, J., Schuck, T., Grossman, M., Clark, C. M., McCluskey, L. F., Miller, B. L., Masliah, E., Mackenzie, I. R., Feldman, H., Feiden, W., Kretzschmar, H. A., Trojanowski, J. Q., & Lee, V. M.-Y. (2006). Ubiquitinated TDP-43 in Frontotemporal Lobar Degeneration and Amyotrophic Lateral Sclerosis. *Science*, *314*(5796), 130–133. https://doi.org/10.1126/science.1134108

Pagani, F., Buratti, E., Stuani, C., & Baralle, F. E. (2003). Missense, Nonsense, and Neutral Mutations Define Juxtaposed Regulatory Elements of Splicing in Cystic Fibrosis Transmembrane Regulator Exon 9. *Journal of Biological Chemistry*, *278*(29), 26580–26588. https://doi.org/10.1074/jbc.M212813200

Panas, M. D., Schulte, T., Thaa, B., Sandalova, T., Kedersha, N., Achour, A., & McInerney, G. M. (2015). Viral and Cellular Proteins Containing FGDF Motifs Bind G3BP to Block Stress Granule Formation. *PLOS Pathogens*, *11*(2), e1004659. https://doi.org/10.1371/journal.ppat.1004659

Patro, R., Duggal, G., Love, M. I., Irizarry, R. A., & Kingsford, C. (2017). Salmon provides fast and bias-aware quantification of transcript expression. *Nature Methods*, *14*(4), 417–419. https://doi.org/10.1038/nmeth.4197

Piatnitskaia, S., Takahashi, M., Kitaura, H., Katsuragi, Y., Kakihana, T., Zhang, L., Kakita, A., Iwakura, Y., Nawa, H., Miura, T., Ikeuchi, T., Hara, T., & Fujii, M. (2019). USP10 is a critical factor for Tau-positive stress granule formation in neuronal cells. *Scientific Reports*, *9*(1), 10591. https://doi.org/10.1038/s41598-019-47033-7

Pickart, C. M. (2001). Mechanisms Underlying Ubiquitination. *Annual Review of Biochemistry*, *70*(1), 503–533. https://doi.org/10.1146/annurev.biochem.70.1.503

Schneider, C. A., Rasband, W. S., & Eliceiri, K. W. (2012). NIH Image to ImageJ: 25 years of image analysis. *Nature Methods*, *9*(7), 671–675. https://doi.org/10.1038/nmeth.2089

Sheehan, C. T., Hampton, T. H., & Madden, D. R. (2022). Tryptophan mutations in G3BP1 tune the stability of a cellular signaling hub by weakening transient interactions with Caprin1 and USP10. *Journal of Biological Chemistry*, *298*(12), 102552. https://doi.org/10.1016/j.jbc.2022.102552

Sidibe, H. (2020). *TDP-43 stabilizes transcripts encoding stress granule protein G3BP1: Potential relevance to ALS/FTD*.

Strong, M. J., Abrahams, S., Goldstein, L. H., Woolley, S., Mclaughlin, P., Snowden, J., Mioshi, E., Roberts-South, A., Benatar, M., HortobáGyi, T., Rosenfeld, J., Silani, V., Ince, P. G., & Turner, M. R. (2017). Amyotrophic lateral sclerosis - frontotemporal spectrum disorder (ALS-FTSD): Revised diagnostic criteria. *Amyotrophic Lateral Sclerosis and Frontotemporal Degeneration*, *18*(3–4), 153–174. https://doi.org/10.1080/21678421.2016.1267768

Takahashi, M., Kitaura, H., Kakita, A., Kakihana, T., Katsuragi, Y., Nameta, M., Zhang, L., Iwakura, Y., Nawa, H., Higuchi, M., Komatsu, M., & Fujii, M. (2018). USP10 Is a Driver of Ubiquitinated Protein Aggregation and Aggresome Formation to Inhibit Apoptosis. *iScience*, *9*, 433–450. https://doi.org/10.1016/j.isci.2018.11.006

Takahashi, M., Kitaura, H., Kakita, A., Kakihana, T., Katsuragi, Y., Onodera, O., Iwakura, Y., Nawa, H., Komatsu, M., & Fujii, M. (2022). USP10 inhibits aberrant cytoplasmic aggregation of TDP-43 by promoting stress granule clearance. *Molecular and Cellular Biology*, MCB.00393-21. https://doi.org/10.1128/MCB.00393-21

Taylor, J. P., Brown, R. H., & Cleveland, D. W. (2016). Decoding ALS: From genes to mechanism. *Nature*, *539*(7628), 197–206. https://doi.org/10.1038/nature20413

Vanden Broeck, L., Kleinberger, G., Chapuis, J., Gistelinck, M., Amouyel, P., Van Broeckhoven, C., Lambert, J.-C., Callaerts, P., & Dermaut, B. (2015). Functional complementation in Drosophila to predict the pathogenicity of TARDBP variants: Evidence for a loss-of-function mechanism. *Neurobiology of Aging*, *36*(2), 1121–1129. https://doi.org/10.1016/j.neurobiolaging.2014.09.001

Vaquero-Garcia, J., Barrera, A., Gazzara, M. R., Gonza, J., Lynch, K. W., & Barash, Y. (n.d.). *A new view of transcriptome complexity and regulation through the lens of local splicing variations*.

Wang, W., Li, L., Lin, W.-L., Dickson, D. W., Petrucelli, L., Zhang, T., & Wang, X. (2013). The ALS disease-associated mutant TDP-43 impairs mitochondrial dynamics and function in motor neurons. *Human Molecular Genetics*, *22*(23), 4706–4719. https://doi.org/10.1093/hmg/ddt319

Wolozin, B., & Ivanov, P. (2019). Stress granules and neurodegeneration. *Nature Reviews Neuroscience*, *20*(11), 649–666. https://doi.org/10.1038/s41583-019-0222-5

Yang, P., Mathieu, C., Kolaitis, R.-M., Zhang, P., Messing, J., Yurtsever, U., Yang, Z., Wu, J., Li, Y., Pan, Q., Yu, J., Martin, E. W., Mittag, T., Kim, H. J., & Taylor, J. P. (2020). G3BP1 Is a Tunable Switch that Triggers Phase Separation to Assemble Stress Granules. *Cell*, *181*(2), 325-345.e28. https://doi.org/10.1016/j.cell.2020.03.046

Yuan, J., Luo, K., Zhang, L., Cheville, J. C., & Lou, Z. (2010). USP10 Regulates p53 Localization and Stability by Deubiquitinating p53. *Cell*, *140*(3), 384–396. https://doi.org/10.1016/j.cell.2009.12.032

Zhang, Y.-J., Caulfield, T., Xu, Y.-F., Gendron, T. F., Hubbard, J., Stetler, C., Sasaguri, H., Whitelaw, E. C., Cai, S., Lee, W. C., & Petrucelli, L. (2013). The dual functions of the extreme N-terminus of TDP-43 in regulating its biological activity and inclusion formation. *Human Molecular Genetics*, *22*(15), 3112–3122. https://doi.org/10.1093/hmg/ddt166

Fig. 1

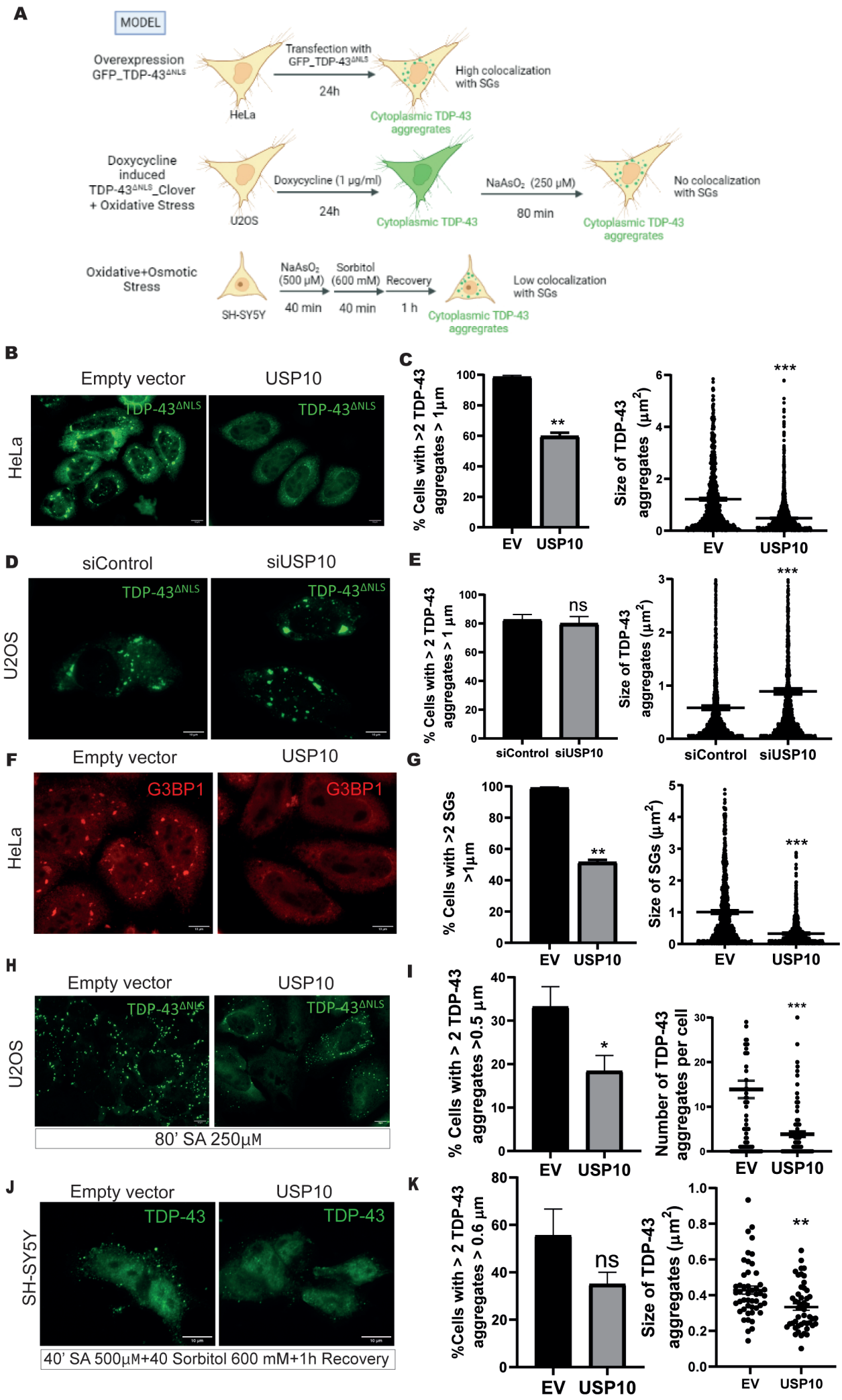
A
MODEL
Overexpression GFP_TDP-43ΔNLS
HeLa
Transfection with GFP_TDP-43ΔNLS
24h
High colocalization with SGs
Cytoplasmic TDP-43 aggregates
Doxycycline induced TDP-43ΔNLS_Clover + Oxidative Stress
U2OS
Doxycycline (1 µg/ml)
24h
Cytoplasmic TDP-43
NaAsO2 (250 µM)
80 min
No colocalization with SGs
Cytoplasmic TDP-43 aggregates
Oxidative+Osmotic Stress
SH-SY5Y
NaAsO2 (500 µM)
40 min
Sorbitol (600 mM)
40 min
Recovery
1 h
Low colocalization with SGs
Cytoplasmic TDP-43 aggregates
B
Empty vector
USP10
HeLa
TDP-43ΔNLS
C
% Cells with >2 TDP-43 aggregates > 1µm
Size of TDP-43 aggregates (µm2)
EV
USP10
D
siControl
siUSP10
U2OS
E
% Cells with > 2 TDP-43 aggregates > 1 µm
Size of TDP-43 aggregates (µm2)
ns
F
G3BP1
G
% Cells with >2 SGs >1µm
Size of SGs (µm2)
H
80' SA 250µM
I
% Cells with > 2 TDP-43 aggregates >0.5 µm
Number of TDP-43 aggregates per cell
J
TDP-43
SH-SY5Y
40' SA 500µM+40 Sorbitol 600 mM+1h Recovery
K
%Cells with > 2 TDP-43 aggregates > 0.6 µm
Size of TDP-43 aggregates (µm2)

Figure 1. TDP-43 cytoplasmic and nuclear aggregation is modulated by USP10.

a) Schematic depiction of the cellular models used to induce cytoplasmic localization and aggregation of TDP-43 (created in BioRender.com): TDP-43$^{\Delta NLS}$ overexpression model, Stress model and inducible TDP-43$^{\Delta NLS}$ expression + Stress model.
b) Representative fluorescence microscope images showing TDP-43 aggregates in HeLa cells 24 hours after co-transfection with GFP-TDP-43$^{\Delta NLS}$ and an empty vector or USP10 (TDP-43$^{\Delta NLS}$ overexpression model). Scale bar: 10 µm.
c) Quantification of the area and percentage of HeLa cells with more than two TDP-43 aggregates bigger than 1 µm after co-transfection with USP10 or co-transfection with an empty vector (EV) control. At least 50 cells per group from 3 independent experiments were analyzed. NS: Not significant; *p<0,01; **p<0,001 by unpaired T-test comparing to the EV control with error bars showing the SEM for all the figure panels.
d) Representative images showing TDP-43 aggregates in U2OS cells 24 hours after co-transfection of GFP-TDP-43$^{\Delta NLS}$ after 72 hours of USP10 downregulation with siRNA. Scale bar: 10 µm.
e) Quantification of the area and percentage of U2OS cells with more than two TDP-43 aggregates bigger than 1 µm after USP10 downregulation with siRNA during 72 h. At least 50 cells per group from 2 independent experiments were analyzed by Mann-Whitney U test compared to siLuciferase control.
f) Representative images showing SGs (labelled with anti-G3BP1 primary antibody in red) in HeLa cells 24 hours after co-transfection of GFP-TDP43$^{\Delta NLS}$ with USP10 or an EV control. Scale bar: 10 µm.
g) Average number of SGs per cell and size of SGs after co-transfection of GFP-TDP43$^{\Delta NLS}$ with USP10 or EV control show a clear reduction in SGs size (-0,6767 ± 0,03459 µm2, p>0,001) and a decrease in the number of cells harbouring SGs (-47,50 ± 1,803, p>0,001) upon USP10 co-transfection when compared to EV. At least 50 cells per group from 2 independent experiments were analyzed and compared by Mann-Whitney U test compared to EV control.
h) Representative fluorescence microscope images showing TDP-43 aggregates in U2OS cells 24 hours after Clover-TDP-43$^{\Delta NLS}$ induction with doxycycline and transfection with an EV or USP10 (TDP-43$^{\Delta NLS}$ overexpression model) upon TDP-43 aggregation induced by incubating the cells with 250 µM sodium arsenite for 80 minutes. Scale bar: 10 µm.
i) Quantification of the number of TDP-43 aggregates per cell and percentage of U2OS cells with more than two TDP-43 aggregates bigger than 0.5 µm after transfection with an USP10 compared to the EV. At least 50 cells per group from 3 independent experiments were analyzed by Mann-Whitney U test compared to EV control.
j) Representative fluorescence microscope images showing TDP-43 aggregates (labelled with anti-TDP-43 primary antibody in green) in SH-SY5Y cells 24 hours after transfection with an EV or USP10. TDP-43 aggregation was induced by incubating the cells consecutively with 500 µM sodium arsenite (40 minutes),

600 mM sorbitol (40 minutes) with 1 hour recovery after the treatment with fresh media. Scale bar: 10 µm.

k) Quantification of the area and percentage of SH-SY5Y cells with more than two TDP-43 aggregates bigger than 0.6 µm after transfection with USP10 when compared to the EV. At least 50 cells per group from 3 independent experiments were analyzed by unpaired T-test compared to control.

Fig. 2

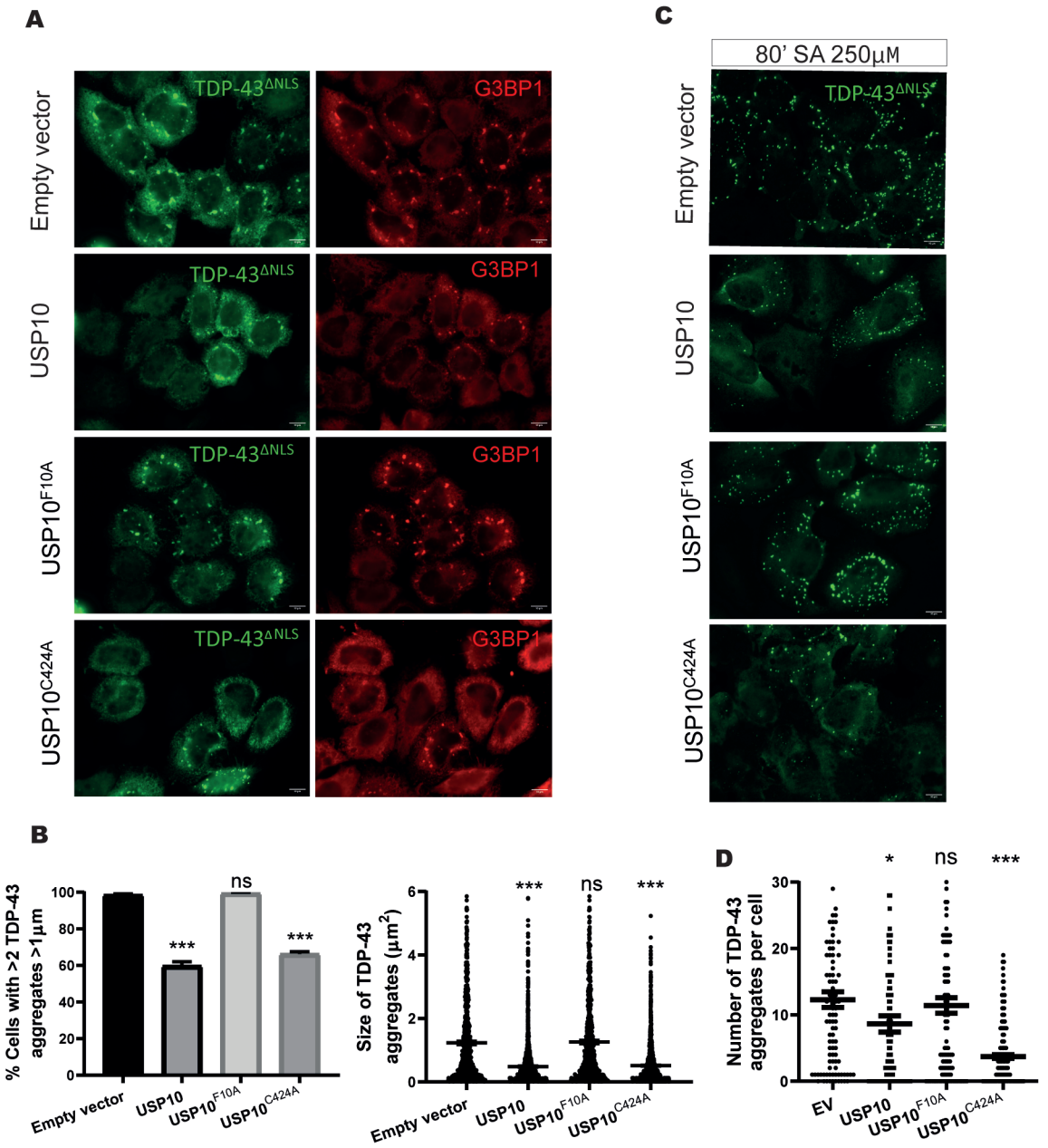
A
Empty vector
USP10
USP10F10A
USP10C424A
TDP-43ΔNLS
G3BP1
C
80' SA 250μM
B
% Cells with >2 TDP-43 aggregates >1μm
Empty vector
USP10
USP10F10A
USP10C424A
***
ns
Size of TDP-43 aggregates (μm2)
D
Number of TDP-43 aggregates per cell
EV
*

Figure 2. USP10 effect on TDP-43 cytoplasmic aggregates is linked to its binding to G3BP1, but independent of its deubiquitinase activity.

a) Representative images of TDP-43 aggregates (green) and stress granules (labelled with anti-G3BP1 primary antibody in red) in HeLa cells 24 hours after co-transfection with GFP-TDP43$^{\Delta NLS}$ and either an EV, USP10 (WT), USP10^{F10A} or USP10^{C424A}. Scale bar: 10 µm.

b) Percentage of HeLa cells with more than two TDP-43 aggregates bigger than 1 µm and quantification of the aggregates size after transfection comparing all constructs to the EV. At least 50 cells per group were analyzed. NS: Not significant; *<0,05; ***p<0,001, by one-way ANOVA with error bars showing the SEM for all the figure panels.

c) Representative images of TDP-43 aggregates (green) in doxycycline inducible TDP-43$^{\Delta NLS}$ U2OS cells 24 hours after doxycycline (1 µg/ml) and 80 minutes after $NaAsO_2$ (250 µM) treatment. Cells were transfected with either an EV, USP10 (WT), USP10^{F10A} or USP10^{C424A}. Scale bar: 10 µm.

d) Quantification of the number of TDP-43 aggregate size after transfection comparing all constructs to the EV. At least 50 cells per group were analyzed. by one-way ANOVA test.

Fig. 3

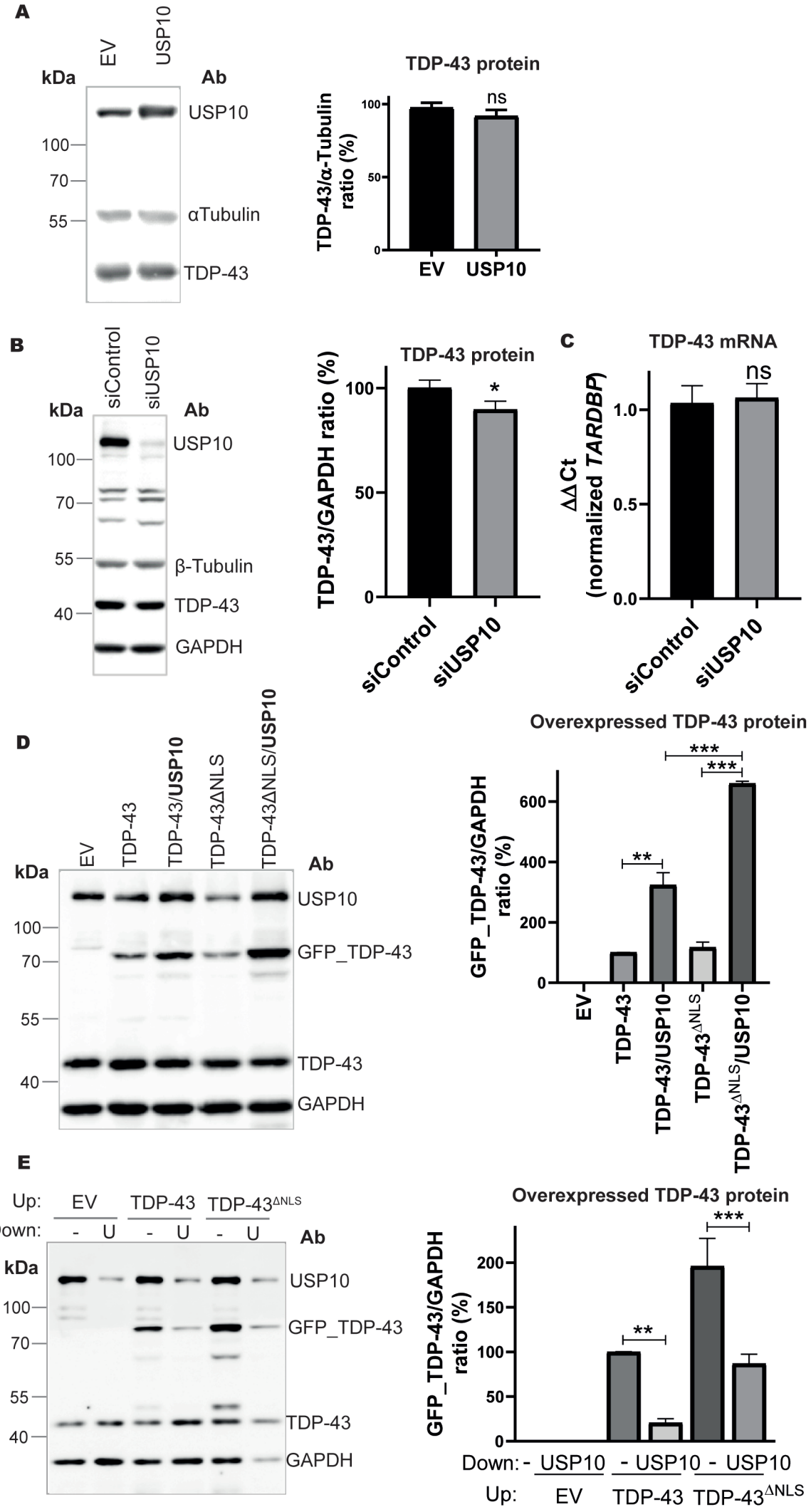
A
EV
USP10
kDa
Ab
USP10
100
70
55
αTubulin
TDP-43
TDP-43 protein
TDP-43/α-Tubulin ratio (%)
ns
EV
USP10
B
siControl
siUSP10
kDa
Ab
USP10
100
70
55
β-Tubulin
40
TDP-43
GAPDH
TDP-43 protein
TDP-43/GAPDH ratio (%)
*
siControl
siUSP10
C
TDP-43 mRNA
ΔΔCt (normalized TARDBP)
ns
siControl
siUSP10
D
EV
TDP-43
TDP-43/USP10
TDP-43ΔNLS
TDP-43ΔNLS/USP10
kDa
Ab
USP10
100
70
GFP_TDP-43
55
TDP-43
40
GAPDH
Overexpressed TDP-43 protein
GFP_TDP-43/GAPDH ratio (%)
***
***
**
EV
TDP-43
TDP-43/USP10
TDP-43ΔNLS
TDP-43ΔNLS/USP10
E
Up: EV TDP-43 TDP-43ΔNLS
Down: - U - U - U
kDa
Ab
USP10
100
70
GFP_TDP-43
55
TDP-43
40
GAPDH
Overexpressed TDP-43 protein
GFP_TDP-43/GAPDH ratio (%)
***
**
Down: - USP10 - USP10 - USP10
Up: EV TDP-43 TDP-43ΔNLS

Figure 3. USP10 controls TDP-43 protein expression

a) Representative image of immunoblot in U2OS cells transfected with USP10 or EV. Specific primary antibodies against USP10, Tubulin, and TDP-43 were used. TDP-43 levels were quantified via densitometry normalized to their loading control (Tubulin). No changes in TDP-43 protein levels were detected following USP10 overexpression compared to the EV by Mann-Whitney U-test ($p=0.8$). N=9. Error bars show the SEM for all panels.
b) Representative image of immunoblot in U2OS cells treated with siRNA against USP10 or siRNA against luciferase (siControl). TDP-43 levels were quantified via densitometry normalized to their loading control (GAPDH). Endogenous TDP-43 protein levels were diminished after USP10 downregulation compared to the siControl. *$p<0.05$, by Mann-Whitney U-test. N=8.
c) Quantification of the relative ΔΔCt expression levels of *TARDBP* transcript, using specific primers and *HPRT* gene as a housekeeping control. The relative mRNA expression of *TARDBP* does not show a significant difference after USP10 downregulation when compared to siControl. N=7.
d) Representative image of immunoblot in U2OS cells transfected with the indicated constructions. Quantification of the volume of GFP-TDP43 bands normalized to their loading control (GAPDH). Pairwise comparisons by one-way ANOVA are depicted. **$p<0.01$; ***$p<0.001$, test. N=3.
e) Representative image of immunoblot in U2OS cells transfected and downregulated with the indicated constructions. Quantification of the volume of GFP-TDP43 bands, normalized to their loading control (GAPDH). Pairwise comparisons by one-way ANOVA are depicted. **$p<0.005$, ***$p<0.001$. N=3.

Fig. 4

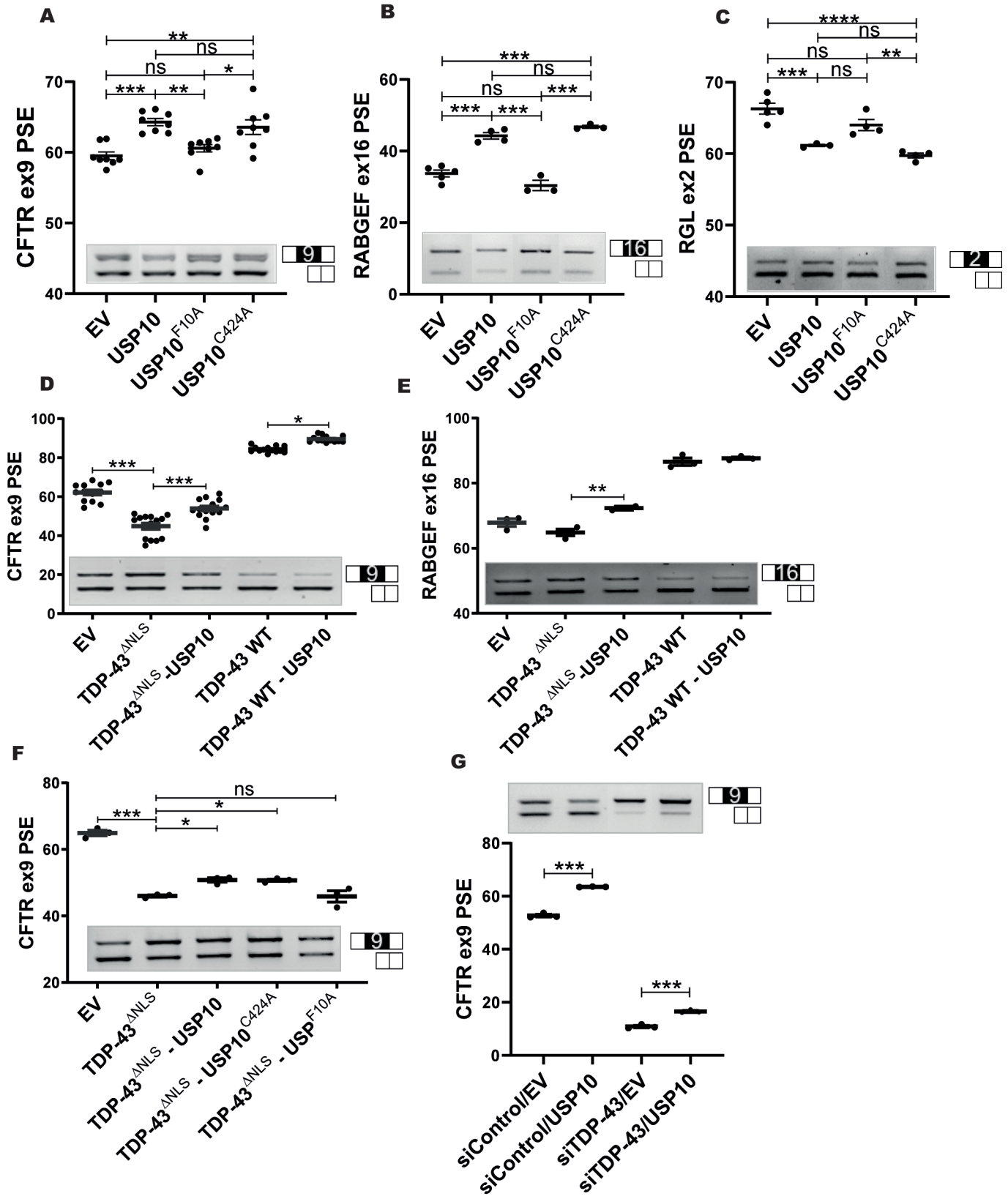
A
CFTR ex9 PSE
EV
USP10
USP10 F10A
USP10 C424A
B
RABGEF ex16 PSE
C
RGL ex2 PSE
D
CFTR ex9 PSE
TDP-43 ΔNLS
TDP-43 ΔNLS -USP10
TDP-43 WT
TDP-43 WT - USP10
E
RABGEF ex16 PSE
F
CFTR ex9 PSE
TDP-43 ΔNLS - USP10
TDP-43 ΔNLS - USP10 C424A
TDP-43 ΔNLS - USP F10A
G
CFTR ex9 PSE
siControl/EV
siControl/USP10
siTDP-43/EV
siTDP-43/USP10

Figure 4. USP10 regulates TDP-43 splicing function

a) Representative image and quantification of the PSE (percentage of splicing exclusion) of the *CFTR* exon 9 minigene. HeLa cells were transfected with the *CFTR* minigene and either an EV, USP10, $USP10^{F10A}$ or $USP10^{C424A}$. Following RT-PCR, the PSE was quantified, and all groups compared to the EV via one-way Anova. N=8. *$p<0.05$, **$p<0.01$, ***$p<0.001$ and error bars represent SEM for all figure panels.
b) Representative image and quantification of the PSE of *RABGEF* exon 16 (b) or *RGL* exon 2 (c). HeLa cells were transfected with either an EV, USP10, $USP10^{F10A}$ or $USP10^{C424A}$. Following RT-PCR, the PSE was quantified, and all groups compared to the EV via one-way Anova. N=4.
d) Representative image and quantification of the PSE of *CFTR* exon 9. HeLa cells were transfected with CFTR minigene and either an EV, GFP-TDP-$43^{\Delta NLS}$ or GFP-TDP-43 WT, and co-transfected or not with USP10. Following RT-PCR, the PSE was quantified, and all groups compared to the EV via one-way Anova. N=4.
e) Representative image and quantification of the PSE of *RABGEF* exon 16. HeLa cells were transfected with *CFTR* minigene and either an EV, GFP-TDP-$43^{\Delta NLS}$ or GFP-TDP-43 WT, and co-transfected or not with USP10. Following RT-PCR, the PSE was quantified, and all groups compared to the EV via one-way Anova. N=4.
f) Representative image and quantification of the PSE of *CFTR* exon 9. HeLa cells were transfected with the *CFTR* minigene and either an EV, GFP-TDP-$43^{\Delta NLS}$ or GFP-TDP-43 WT, and co-transfected or not with USP10. Following RT-PCR, the PSE was quantified, and all groups compared to the EV via one-way Anova. N=4.
g) Representative image and quantification of the PSE of *CFTR* exon 9. U2OS cells were co-transfected with siRNA against TDP-43 or luciferase as a negative control together with either EV or USP10. Following RT-PCR, the PSE was quantified, and all groups compared to the EV via one-way Anova. N=3.

Fig. 5

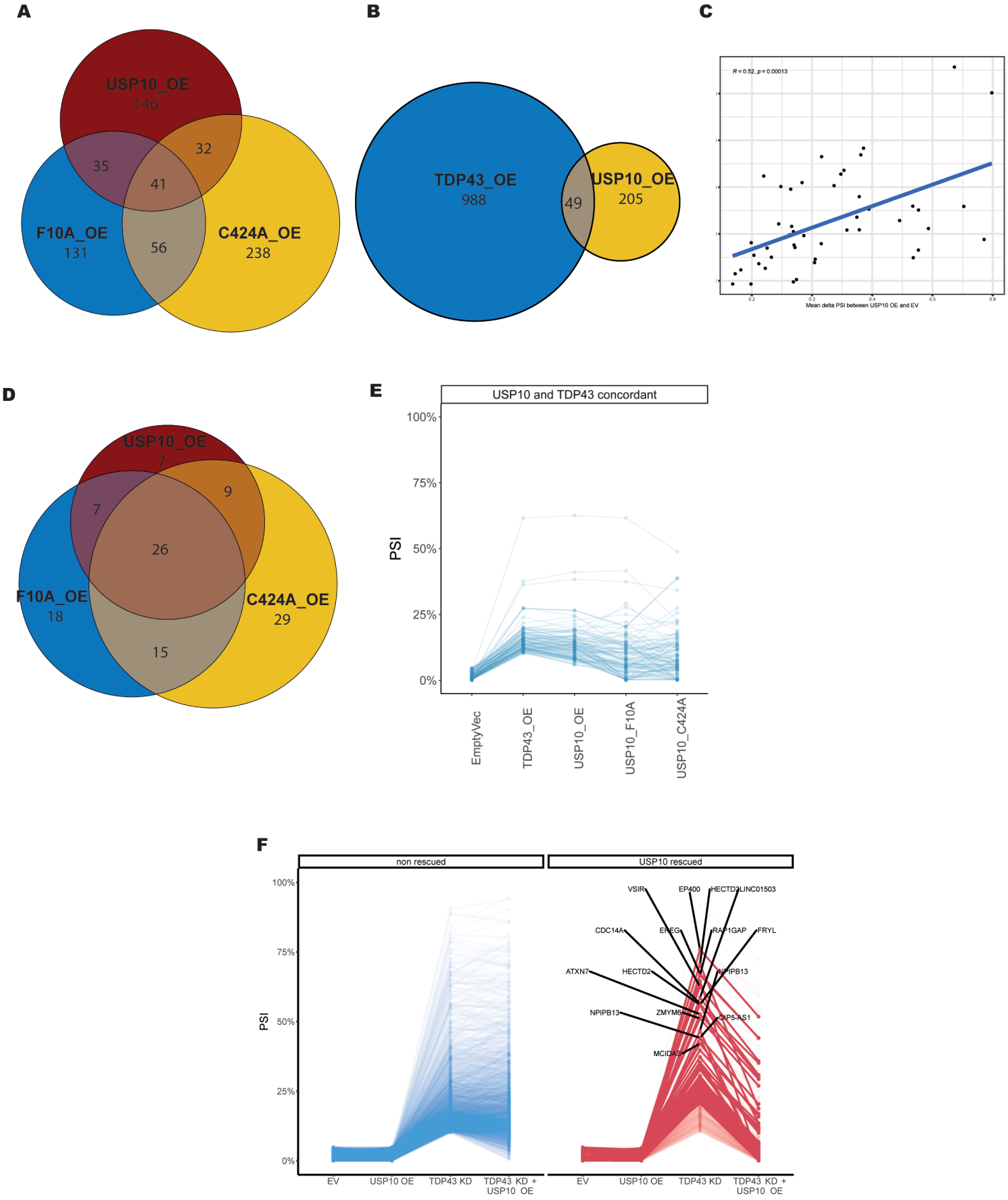
A
USP10_OE
146
32
35
41
F10A_OE
131
56
C424A_OE
238
B
TDP43_OE
988
49
USP10_OE
205
C
R = 0.52, p = 0.00013
Mean delta PSI between USP10 OE and EV
D
USP10_OE
7
9
7
26
F10A_OE
18
C424A_OE
29
15
E
USP10 and TDP43 concordant
PSI
100%
75%
50%
25%
0%
EmptyVec
TDP43_OE
USP10_OE
USP10_F10A
USP10_C424A
F
non rescued
USP10 rescued
PSI
100%
75%
50%
25%
0%
VSIR
EP400
HECTD2
LINC01503
CDC14A
EPEG
RAP1GAP
FRYL
ATXN7
HECTD2
NPIPB13
NPIPB13
ZMYM6
GIP5-AS1
MCIDAS
EV
USP10 OE
TDP43 KD
TDP43 KD + USP10 OE
EV
USP10 OE
TDP43 KD
TDP43 KD + USP10 OE

Figure 5: USP10 regulates alternative splicing

a) Venn diagram showing the number of splice junctions modified and shared by each USP10 condition in HeLa cells. USP10_OE: USP10 WT overexpression; F10A_OE: USP10 F10A overexpression; C424A_OE: USP10 C424A overexpression

b) Venn diagram showing the number of overlapping splicing junctions that are significantly changed upon transfection of HeLa cells with TDP-43 with those affected by $USP10^{WT}$.

c) Correlation between the delta PSI of different splicing events after transfection of HeLa cells with TDP-43 or $USP10^{WT}$. The Pearson's correlation coefficient (R) and the p-value are indicated.

d) Venn diagram showing the number of splicing events overlapping between the three USP10 conditions specifically for the splicing events shared between TDP-43 and USP10.

e) Representation of the PSI changes specifically for the splicing events shared between TDP-43 and USP10 in all conditions: EV, TDP-43, $USP10^{WT}$, $USP10^{F10A}$ or $USP10^{C424A}$. Each line represents a shared splicing event for all conditions.

f) Representation of the changes in the PSI of cryptic exons that are rescued (red) or not (blue) by the overexpression of USP10 after TDP-43 downregulation in HeLa cells. A subset of the most changed event is also annotated with the gene names.

Fig. 6

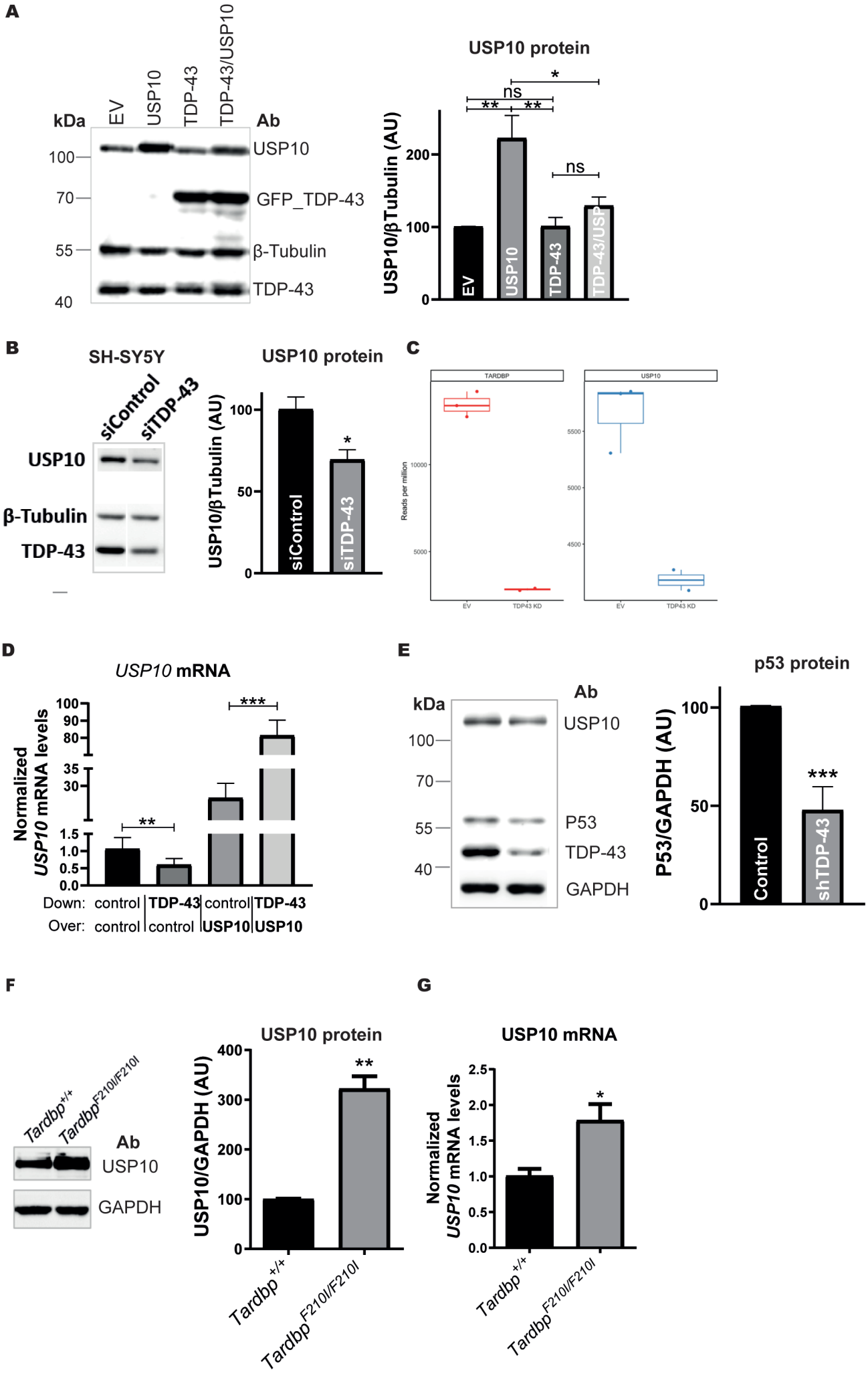
A
kDa
EV
USP10
TDP-43
TDP-43/USP10
Ab
100
70
55
40
USP10
GFP_TDP-43
β-Tubulin
TDP-43
USP10 protein
USP10/βTubulin (AU)
ns
*
**
**
ns
200
100
0
EV
USP10
TDP-43
TDP-43/USP
B
SH-SY5Y
siControl
siTDP-43
USP10
β-Tubulin
TDP-43
USP10 protein
USP10/βTubulin (AU)
100
50
0
*
siControl
siTDP-43
C
TARDBP
USP10
Reads per million
10000
5000
5500
5000
4500
EV
TDP43 KD
EV
TDP43 KD
D
USP10 mRNA
Normalized USP10 mRNA levels
100
90
80
35
30
1.5
1.0
0.5
0.0
**
***
Down: control TDP-43 control TDP-43
Over: control control USP10 USP10
E
kDa
Ab
100
70
55
40
USP10
P53
TDP-43
GAPDH
p53 protein
P53/GAPDH (AU)
100
50
0
***
Control
shTDP-43
F
Tardbp+/+
TardbpF210I/F210I
Ab
USP10
GAPDH
USP10 protein
USP10/GAPDH (AU)
400
300
200
100
0
**
Tardbp+/+
TardbpF210I/F210I
G
USP10 mRNA
Normalized USP10 mRNA levels
2.5
2.0
1.5
1.0
0.5
0.0
*
Tardbp+/+
TardbpF210I/F210I

Figure 6. TDP-43 controls USP10 expression

a) Representative image of immunoblot and quantification of HeLa cells transfected with either USP10, TDP-43 or EV alone or the combination (TDP-43/USP10). Quantification of USP10 bands by densitometry was normalized to their loading control (β-Tubulin). All groups were compared pairwise via one-way Anova. N=3. *p<0.05, **p<0.01, ***p<0.001 and error bars represent SEM for all figure panels.
b) Representative image of immunoblot and quantification of SH-SY5Y downregulated for 72 h. with either siRNA against TDP-43 or a negative control (siControl). Quantification of USP10 bands by densitometry was normalized to their loading control (β-Tubulin). USP10 protein was reduced by -30.83 ± 9.58 upon TDP-43 downregulation (*p<0,05 by unpaired T test to control). N=3.
c) Quantification (reads per million) of *TARDBP* and *USP10* transcripts by RNA-seq analysis after TDP-43 overexpression in HeLa cells.
d) Quantification of the relative ΔΔCt expression levels of *USP10*, using specific primers and *HPRT* gene as housekeeping control, in U2OS cells transfected with either a siTDP-43 or a negative control (siControl), and also in cells co-transfected with either USP10 or an EV control in the context of siTDP-43 or siControl. *USP10* mRNA levels were significantly reduced upon TDP-43 downregulation when compared to siControl. In turn, *USP10* transcript levels were further increased in cells co-transfected with USP10 in the context of TDP-43 downregulation when compared to the *USP10* levels reached by overexpression in the context of the siControl. (*p<0.05, **p<0.01 by unpaired T test to control). N=3 for both set of experiments.
e) Representative image of immunoblot of an inducible SK-N-BE cell line expressing shRNA against TDP-43 upon doxycycline, treated or not for 72h. Quantification of p53 bands by densitometry was normalized to their loading control (GAPDH). p53 protein was reduced a -52.73 ± 11.79 upon TDP-43 downregulation when compared to the doxycycline untreated by Mann Whitney U test. N=8.
f) Representative image of immunoblot from *Tardbp*$^{F210I/F210I}$ MEFs versus *Tardbp*$^{+/+}$ control. Quantification of p53 bands by densitometry was normalized to their loading control (GAPDH). USP10 protein levels are increased a 322.3 % in fibroblasts homozygous for the *Tardbp*$^{F210I/F210I}$ mutation when compared to controls (**p<0.01, by unpaired T test to WT). N=5.
g) Quantification of the relative ΔΔCt expression levels of *Usp10* from *Tardbp*$^{F210I/F210I}$ MEFs and controls using specific primers and *S16* gene as housekeeping control. The relative expression of *USP10* is increased by 0.7762 units in *Tardbp*$^{F210/F210I}$ relative to *Tardbp*$^{+/+}$ by unpaired T-test (*p<0.05). N=3.

Fig. 7

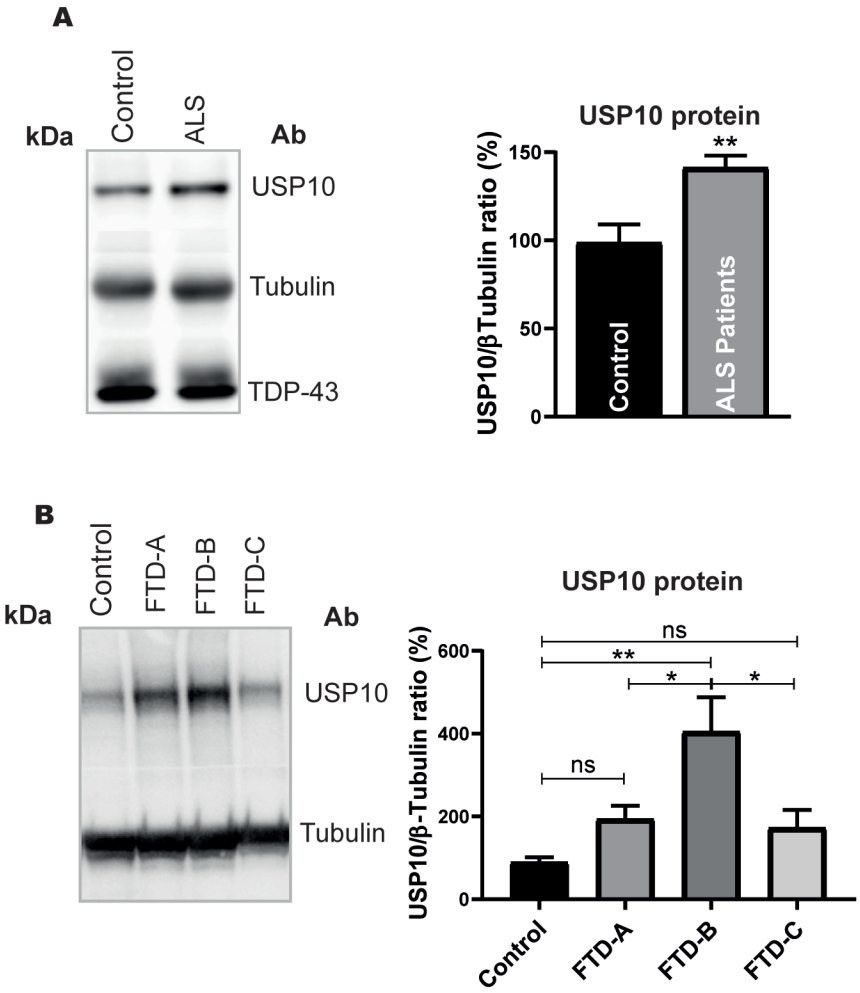
A
kDa
Control
ALS
Ab
USP10
Tubulin
TDP-43
USP10 protein
USP10/βTubulin ratio (%)
150
100
50
0
**
Control
ALS Patients
B
kDa
Control
FTD-A
FTD-B
FTD-C
Ab
USP10
Tubulin
USP10 protein
USP10/β-Tubulin ratio (%)
600
400
200
0
ns
**
*
*
ns
Control
FTD-A
FTD-B
FTD-C

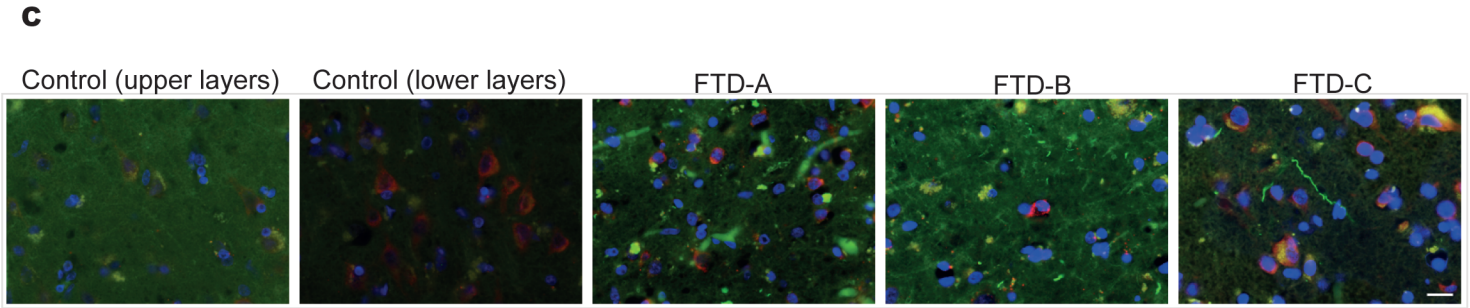
C
Control (upper layers)
Control (lower layers)
FTD-A
FTD-B
FTD-C

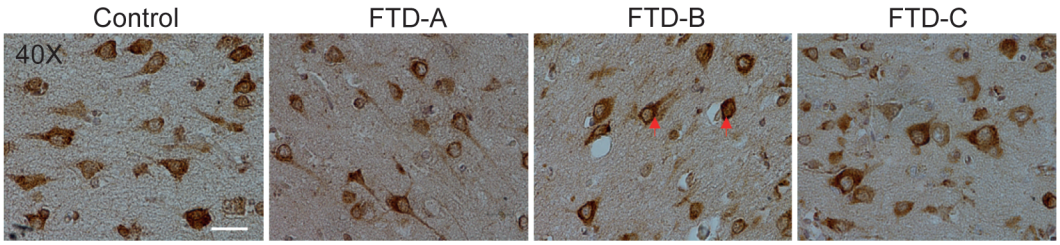
D
Control
FTD-A
FTD-B
FTD-C
40X

Figure 7. USP10 is affected in TDP-43 proteinopathies.

a) Representative image of immunoblot and quantification of USP10 in protein lysates of motor cortex from ALS patients and controls. Quantification of USP10 bands by densitometry was normalized to their loading control (Tubulin). Controls (98.71 ± 10.35%); ALS (141.3 ± 6.711%), compared by Mann-Whitney U-test. *p<0,01, and error bars show SEM for all panels. Samples from 5 patients and 5 controls were used.
b) Representative image of immunoblots from frontal cortex protein lysates from FTD patients and controls and quantification of USP10 bands by densitometry normalized to their loading control (Tubulin), separating the patient samples by the different FTLD-TDP pathology subtypes. Control (89.36 ± 11.90 %); FTD-A (193.7 ± 32.00 %); FTD-B (404.8 ± 82.88 %); FTD-C (172.1 ± 43.83 %). USP10 levels were particularly increased in samples from patients with TDP-43 type B pathology, where there is a 315.4 % increase in USP10 compared to controls (p<0.01). Samples from 3 patients per pathology subtype and 3 controls were used.
c) Representative immunofluorescence images of post-mortem slices of frontal cortex samples from FTD patients. Samples from different cortical layers of healthy patients were used as controls. Primary anti-pTDP-43 labelled in green, and anti-USP10 in red were used, with nuclei labelled with DAPI (Blue). Figure shows the merged images from the three channels. Red arrows show USP10 cytoplasmic accumulations in neurons. Scale bar: 50 µm. Images of samples from 5 healthy controls and 5 patients per pathology subtype were analysed.

d) Representative immunohistochemistry images of USP10 in post-mortem slices of frontal cortex samples from FTD patients and healthy patients (used as controls). A primary anti-USP10 antibody was used with a biotinylated secondary revealed by hydrogen peroxidase-activated diaminobenzidine (DAB) solution. Red arrows show increased USP10 immunoreactivity in the cytoplasm of some neurons. Scale bar: 50 µm. Images of samples from 5 healthy controls and 5 patients per pathology subtype were analysed.